THERMAL AND MECHANICAL BEHAVIOUR OF THE OROGENIC MIDDLE CRUST DURING THE SYN- TO LATE-OROGENIC EVOLUTION OF THE VARISCAN ROOT ZONE, BOHEMIAN MASSIF

B. PETRI[1,2], P. ŠTÍPSKÁ[1,3], E. SKRZYPEK[4], K. SCHULMANN[1,3], M. CORSINI[5], and J. FRANĚK[6]

[1]*Ecole et Observatoire des Sciences de la Terre, Institut de Physique du Globe de Strasbourg – CNRS UMR7516, Université de Strasbourg, 1 rue Blessig, F−67084, Strasbourg Cedex, France*
[2]*Vrije Universiteit, Department of Petrology, de Boelelaan 1085, 1081HV Amsterdam, The Netherlands*
[3]*Center for Lithospheric Research, Czech Geological Survey, 11821 Praha 1, Czech Republic*
[4]*Department of Geology and Mineralogy, Graduate School of Science, Kyoto University, Kitashirakawa Oiwake−cho, Sakyo−ku, 606−8502 Kyoto, Japan*
[5]*Université de Nice Sophia−Antipolis, GeoAzur – CNRS UMR 6526, Parc Valrose, Bât Sciences Naturelles, F−06108, Nice Cedex, France*
[6]*Czech Geological Survey, Klárov 3,CZ−118 21 Prague, Czech Republic*

Short title: Behaviour of the Variscan middle crust

REFERENCE

Petri B., Štípská P., Skrzypek E., Schulmann K., Corsini M. & Franěk J., 2014. Thermal and mechanical behavior of the orogenic middle crust during the syn- to late-orogenic evolution of the Variscan root zone, Bohemian Massif. Journal of Metamorphic Geology, 32 (6), 599-626. DOI:10.1111/jmg.12081

ABSTRACT

We combine structural observations, petrological data and ^{40}Ar–^{39}Ar ages for a stack of amphibolite-facies metasedimentary units that rims high-pressure (HP) granulite-facies felsic bodies exposed in the southern Bohemian Massif. The partly migmatitic Varied and Monotonous units, and the underlying Kaplice unit show a continuity of structures that are also observed in the adjacent Blanský les HP granulite body. They all exhibit an earlier NE−SW striking and steeply NW-dipping foliation (S3) which is transposed into a moderately NW-dipping foliation (S4). In both the Varied and Monotonous units, the S3 and S4 foliations are characterized by a Sil–Bt–Pl–Kfs–Qtz–Ilm±Grt assemblage, with occurrences of post-D4 andalusite, cordierite and muscovite. In the Monotonous unit, minute inclusions of garnet, kyanite, sillimanite and biotite are additionally found in plagioclase from a probable leucosome parallel to S3. The Kaplice unit shows rare

staurolite and kyanite relicts, a Sil–Ms–Bt–Pl–Qtz±Grt assemblage associated with S3, retrogressed garnet−staurolite aggregates during the development of S4, and post-D4 andalusite, cordierite and secondary muscovite. Mineral equilibria modelling for representative samples indicates that the Varied unit records conditions higher than ~7 kbar at 725 °C during the transition from S3 to S4, followed by a $P-T$ decrease from ~5.5 kbar/750 °C to ~4.5 kbar/700 °C. The Monotonous unit shows evidence of partial melting in the S3 fabric at $P-T$ above ~8 kbar at 740–830 °C and a subsequent $P-T$ decrease to 4.5–5 kbar/700°C. The Kaplice unit preserves an initial medium-pressure prograde path associated with the development of S3 reaching peak $P-T$ of ~6.5 kbar/640 °C. The subsequent retrograde path records 4.5 kbar/660 °C during the development of S4. ^{40}Ar–^{39}Ar geochronology shows that amphibole and biotite ages cluster at *c*. 340 Ma close to the HP granulite, whereas adjacent metasedimentary rocks preserve *c.* 340 Ma amphibole ages, but biotite and muscovite ages range between *c*. 318 and *c*. 300 Ma. The $P-T$ conditions associated with S3 imply an overturned section of the orogenic middle crust. The shared structural evolution indicates that all mid-crustal units are involved in the large-scale folding cored by HP granulites. The retrograde $P–T$ paths associated with S4 are interpreted as a result of a ductile thinning of the orogenic crust at a mid-crustal level. The ^{40}Ar–^{39}Ar ages overlap with U–Pb zircon ages in and around the HP granulite bodies, suggesting a short duration for the ductile thinning event. The post-ductile thinning late-orogenic emplacement of the South Bohemian plutonic complex is responsible for a re-heating of the stacked units, reopening of argon system in micas and a tilting of the S4 foliation to its present-day orientation.

Key words: $P-T-t-d$ path, mineral equilibria modelling, thermochronology, burial and exhumation, Moldanubian domain.

INTRODUCTION

The thickened continental crust of orogens may be divided into three discrete levels: the upper, middle and lower orogenic crust. In the Bohemian Massif, the upper crust corresponds mostly to sedimentary material metamorphosed at low-grade conditions. As a result, the pressure−temperature−time−deformation ($P-T-t-d$) evolution is well preserved, and the burial history has been well characterised (e.g. Ahrendt *et al*., 1983). The lower crust refers to relatively high-pressure rocks that are formed at depths exceeding the thickness of equilibrated continental crust. Although the early stages of the metamorphic evolution of the lower crust may be erased by high-grade conditions, the large number of studies dedicated to this crustal level has significantly improved understanding of the $P-T-t-d$ evolution and, especially, the exhumation history of it (e.g. Štípská *et al*., 2004). The middle crust represents the intermediate layer in which parts of the upper crust may be buried and into which parts of the lower crust may be exhumed (e.g. Grujic *et al*., 2011). As such, the thermo-mechanical behaviour of the orogenic

middle crust represents a key element for constraining burial and exhumation processes in the orogens.

However, reconstructing the *P*−*T*−*t*−*d* evolution of the middle crust is rendered difficult by the superposition of several deformation and metamorphic events. The middle orogenic crust shows metamorphism ranging from upper greenschist- to upper amphibolite-facies conditions, but wide zones of partial melting are described at various depths (e.g. Nelson *et al*., 1996). Such high temperature zones may be responsible for a partial to complete resetting of the earlier *P*−*T* records. It follows that *P*−*T* estimates are rarely linked with structural or temporal constraints. Therefore, a first goal of this study is to reconstruct a detailed *P*−*T*−*t*−*d* evolution for the middle crust.

With respect to the upper and lower crust, the middle crust may behave in three different ways: (i) it may share the evolution of both the upper and lower crust if there is vertical coupling between all three units (e.g. Klepeis *et al*., 2004); (ii) it may form a coherent unit with the lower crust, but be decoupled from an overlying upper crustal lid (Wegman, 1935); or, (iii) it may be fully decoupled from the other two crustal levels, as in the channel flow model (Beaumont *et al*., 2001). Because the thermo-mechanical evolution of the middle crust is rarely related to that of the surrounding crustal levels, a second goal of this study is to identify the degree of coupling between the upper, middle and lower crust.

An adequate area to address these issues is the Bohemian Massif where fragments of the Variscan upper, middle and lower orogenic crust are exposed (Franke, 2000; Schulmann *et al*., 2009). The upper crustal Teplá-Barrandian domain, owing to a moderate metamorphic overprint, preserves a well-documented succession of Cadomian and Variscan tectono-thermal events (Timmermann, 2006; Zulauf, 1997). In the mid- and lower crustal Moldanubian domain, previous studies focused on the *P*−*T*−*t*−*d* evolution of high-pressure (HP) granulites, eclogites and peridotites belonging to the orogenic lower crust (Carswell & O'Brien, 1993; Medaris *et al.*, 2006; O'Brien & Vrána, 1995). However, the tectono-metamorphic evolution of mid-crustal rocks which surround the lower crustal exposures remains unconstrained, especially because the superposition of tectono-metamorphic events makes such a task challenging.

To fill this gap in knowledge, we constrain the *P*−*T*−*t*−*d* evolution of three mid-crustal metasedimentary units along a section exposed in the Central Bohemian Massif. The stack of units is located around the largest outcrop of lower crustal rocks in the Bohemian Massif, the Blanský les granulite body. We apply a structural analysis in order to define the relative succession of orogenic fabrics, and decipher the *P*−*T*−*d* path of metasedimentary rocks using crystallization−deformation relationships and mineral equilibria modelling. Time constraints on the thermal events affecting the middle crust are derived from ^{40}Ar–^{39}Ar dating on biotite and amphibole, combined with a synthesis of published ages. Finally, the *P*−*T*−*t*−*d* evolution is related to those previously proposed for the neighbouring upper and lower orogenic levels.

GEOLOGICAL SETTING

The Bohemian massif

The Bohemian massif is located in the northeastern part of the European Variscan Belt (Fig. 1a). From NW to SE, it is classically divided into four litho-tectonic domains (Fig. 1b): the Saxothuringian, Teplá−Barrandian, Moldanubian and Brunovistulian domains (e.g. Schulmann *et al.*, 2009). The Neoproterozoic to Early Palaeozoic Teplá−Barrandian domain was recently interpreted as the superstructure of the Carboniferous thickened orogenic root (Maierová *et al.*, 2014; Schulmann *et al.*, 2009). This supracrustal unit is bordered to the NW by the subducted Neoproterozoic Saxothuringian basement and its Lower Palaeozoic sedimentary cover, and to the SE by the underlying Moldanubian domain corresponding to the orogenic infrastructure. The southeastern border of the Teplá−Barrandian is intruded by Late Devonian (380–365 Ma, Košler *et al.*, 1993) to Early Carboniferous magmatic rocks (354–337 Ma, Janoušek & Gerdes, 2003) of the Central Bohemian plutonic complex, which is regarded as a magmatic arc associated with the SE−directed subduction of the Saxothuringian domain (Konopásek & Schulmann, 2005; Žák *et al.*, 2005).

The Moldanubian domain

The Moldanubian domain is divided into the high-grade Gföhl and medium-grade Drosendorf units, which record contrasting $P-T$ evolutions (Tollmann, 1982). This domain is intruded by numerous ultra-potassic plutons, and by the late- to post-tectonic peraluminous South Bohemian plutonic complex. The Gföhl unit is composed of migmatitic orthogneiss, felsic to intermediate granulite, eclogite and peridotite. These high-grade rocks preserve Precambrian to Early Ordovician protolith ages (Friedl *et al.*, 2004; Janoušek *et al.*, 2004; Schulmann *et al.*, 2005). Eclogites and HP granulites experienced an initial HP-UHP metamorphic event (e.g. Faryad *et al.*, 2010; Kotková *et al.*, 2010; Medaris *et al.*, 1998; Nahodilová *et al.*, 2014) followed by granulite-facies conditions estimated at 14−20 kbar and 800−950 °C (Faryad *et al.*, 2010; Franěk *et al.*, 2011a). Amphibolite facies retrogression (6−8 kbar, 600−800°C) occurred during the exhumation of the granulites to mid-crustal levels (Franěk *et al.*, 2011a; Lexa *et al.*, 2011). Peak temperatures during granulite-facies metamorphism were estimated to occur between *c.* 360 and *c.* 340 Ma on the basis of numerous U−Pb zircon ages (Kotková, 1993; Willner *et al.*, 1997). The U−Pb zircon and monazite ages of 340–330 Ma obtained from the retrogressed granulites and the associated syntectonic granitoids are interpreted to date granulite exhumation (Kotková *et al.*, 2010; Štípská *et al.*, 2004; Tajčmanová *et al.*, 2006; Verner *et al.*, 2008). Cooling of the granulite massifs is constrained to the interval 340−330 Ma by a range of amphibole and biotite $^{40}Ar-^{39}Ar$ ages (Kotková *et al.*, 1996; Kröner & Willner, 1998).

The Drosendorf unit is divided into the Varied and Monotonous units. The Varied unit is composed of Early Palaeozoic paragneiss with amphibolite, marble, calc-silicate

rocks and meta-quartzite, while the Monotonous unit is dominated by metagraywacke, metapelite and quartzite. The youngest detrital zircons from the metasedimentary rocks are Early Ordovician for the Monotonous and Mid to Late Devonian for the Varied unit (Košler *et al.*, 2014). This suggests that filling of the sedimentary basins forming the precursors of the Monotonous and Varied units occured in Palaeozoic times. Kyanite-bearing paragneiss in the Varied unit records peak *P*−*T* conditions of 8−9 kbar and 610−700 °C, followed by re-equilibration in the sillimanite stability field at 4−6 kbar and 600−650 °C (e.g. Petrakakis, 1997; Pitra & Guiraud, 1996; Racek *et al.*, 2006; Štípská *et al.*, 2008). Paragneiss in the Monotonous unit, which locally hosts eclogite bodies, is characterized by a biotite−sillimanite assemblage and evidence of significant partial melting. Peak *P*−*T* conditions in paragneiss are estimated at 7−10 kbar and 700−800°C (Scheuvens, 2002), and were followed by retrogression to 6−7 kbar and 620−740°C (Tropper *et al.*, 2006). Additionally, the Monotonous unit is known to record the thermal influence of the large Carboniferous intrusions (330−310 Ma), which generate *P*−*T* conditions of 4.5–6 kbar and 600–720 °C (Petrakakis, 1997; Vrána *et al.*, 2005).

Lithologies surrounding the Blanský les granulite massif

This study focuses on the metasedimentary sequences of the Moldanubian domain located in the area limited by the Blanský les and the Křišťanov granulite massifs to the W, and the South Bohemian plutonic complex to the SE (Fig. 2a). The westernmost Varied unit consists of migmatitic metapelite, marble and amphibolite with a Lower Palaeozoic protolith age, as indicated by Re−Os dating of marble (Drábek & Stein, 2003). It hosts a 2.1 Ga-old orthogneiss body deformed at amphibolite-facies conditions during the Carboniferous (Patočka *et al.*, 2003; Wendt *et al.*, 1993). Recent geochemical and geochronological studies from south Bohemia (Janoušek *et al.*, 2008; Košler *et al.*, 2014) indicate that the volcanism/sedimentation of the Varied unit occurred during Early Palaeozoic intracontinental rifting, which lasted until the Mid to Late Devonian. The Monotonous unit occurs as a central NE−SW trending belt and is mostly composed of migmatitic paragneiss with a few eclogite bodies for which *P*−*T* conditions of 20−25 kbar and 750°C are reported (Faryad *et al.*, 2006; O'Brien & Vrána, 1995). The Kaplice unit occurs to the SE and is dominated by muscovite-bearing micaschist, locally containing garnet, staurolite and cordierite. It is crosscut by several younger granodiorite dykes connected to the southern Freistadt granodioritic pluton, which was emplaced along the Kaplice fault zone at *c.* 300 Ma (Vrána *et al.*, 2005).

The South Bohemian plutonic complex consists of granitoids emplaced between *c.* 330 and *c.* 300 Ma. According to Gerdes *et al.* (2000), ~80% of the surface of the complex is occupied by the Weinsberg (331−323 Ma) and Eisgarn types (328−327 Ma). The more heterogeneous Freistadt-type consists of a granodioritic to granitic suite emplaced between *c.* 317 and *c.* 300 Ma.

STRUCTURAL EVOLUTION

Previous structural studies of the southern Moldanubian domain reveal a polyphase deformation history (Lobkowicz *et al.*, 1996; Vrána, 1979; Vrána & Bártek, 2005). In the granulite massifs surrounding the study area, a succession of four deformation events is documented (Franěk *et al.*, 2011a). The S1 and S2 foliations are rare, and the present-day antiformal shape of the granulite bodies mostly reflects the superposition of an early D3 vertical shortening, a late D3 upright folding, and a subsequent D4 vertical shortening that becomes more intense to the West (Franěk *et al.*, 2006; 2011a). The resulting S3 and S4 fabrics are recognized in both the granulite and surrounding metasedimentary rocks (Franěk *et al.*, 2011a). We similarly observe a structural continuity between the granulite massifs and the surrounding units for the S3 and S4 fabrics (Fig. 3). Accordingly, we decided to follow the structural scheme defined by Franěk *et al.* (2011a) to facilitate the discussion of structural relationships between these two domains.

In the Varied and Monotonous units, the first macroscopically visible structure is the regional foliation S3. It is defined by a compositional layering, an alternation of leucosomes and melanosomes, and a shape-preferred orientation of biotite and mineral aggregates (Fig. 4a,c). It is exceptionally preserved in the southwestern part of the study area (Fig. 2b), where the S3 foliation strikes NE−SW and dips steeply to the NW or locally to the SE (Figs. 2 & 3). In the Kaplice unit, the S3 foliation is defined by a compositional layering, a preferred orientation of muscovite and biotite and elongated quartz segregations. Rare leucosomes parallel to S3 are also observed in paragneiss (Fig. 4e,f). The S3 foliation is preserved in few low-strain domains in the southern part of the Kaplice unit; it trends NE−SW and commonly dips at a steep angle to the NW (Fig. 2b).

In the Varied, Monotonous and Kaplice units, the steep S3 foliation is affected by open to isoclinal recumbent F4 folds with NE–SW trending hinges and axial planes dipping at a moderate angle to the NW (Figs. 2, 3 & 4a). The F4 folding commonly leads to an almost entire transposition of the S3 fabric into a new continuous metamorphic foliation S4, though rare relicts of S3 occur as rootless folds. The transposition is associated with the development of numerous pinch-and-swell structures where rectangular boudins of quartzite lie in marble layers (Fig. 4b). In the Varied and Monotonous units, the S4 foliation is migmatitic and mylonitic; it is defined by a compositional layering, elongated leucosomes and a preferred orientation of biotite in paragneiss. Coarse-grained leucosomes in interboudin partitions associated with the S4 foliation document anatexis during the D4 deformation (Fig. 4d). In places, the microscopic observation of leucosomes reveals a solid-state recrystallization of quartz and feldspars, indicating that the D4 deformation also continued to subsolidus conditions. In general, the S4 fabric is NE−SW striking and gently to moderately NW-dipping. The general trend of the S4 fabric is locally perturbed by large-scale open flexures affecting both the Monotonous and Varied units along the southern edge of the Blanský les granulite massif (Fig. 2b).

In the Kaplice unit, the S4 foliation is marked by elongated quartz segregations and by the preferred orientation of muscovite and biotite in micaschist. Leucosomes oriented parallel to S4 locally occur in paragneiss. Cordierite, kyanite, sillimanite and andalusite, commonly up to several centimeters in size, occur at the margins of quartz segregations (Fig. 6c,d). In this area, the S4 fabric strikes NE−SW and moderately dips to the NW (Fig. 2b). In the Kaplice unit, the S4 foliation in micaschist is affected by cm-scale chevron folds F5 with E−W trending hinges and subvertical axial planes. This late F5 folding locally generates a weak subvertical cleavage S5 (Fig. 4g).

PETROGRAPHY AND MINERAL CHEMISTRY

To characterize the *P*−*T*−*d* evolution, several oriented thin sections of paragneiss and micaschist were studied in the three units. For each unit, one representative sample was selected for analysis of mineral compositions (see Appendix for analytical procedure). Microscopic observations are illustrated in Figs. 5 & 6, and the interpretation of crystallization−deformation relationships is presented in Fig. 7. Representative mineral analyses are summarized in Table 1 and garnet chemistry is shown in Fig. 8. Mineral and end-member abbreviations follow IUGS recommendations (Siivola & Schmid, 2007). Compositional variables in minerals are defined as follows: *X*Fe = Fe/(Fe+Mg), *Alm* = Fe^{2+}/(Fe^{2+}+Mg+Ca+Mn), *Prp* = Mg/(Fe^{2+}+Mg+Ca+Mn), *Grs* = Ca/(Fe^{2+}+Mg+Ca+Mn), *Sps* = Mn/(Fe^{2+}+Mg+Ca+Mn), *Ab* = Na/(Na+Ca+K), *An* = Ca/(Na+Ca+K), *Or* = K/(Na+Ca+K) for measured compositions; *x*(Grt,St) = Fe/(Fe+Mg)*100, *alm*(Grt) = Fe^{2+}/(Fe^{2+}+Mg+Ca+Mn), *prp*(Grt) = Mg/(Fe^{2+}+Mg+Ca+Mn), *grs*(Grt) = Ca/(Fe^{2+}+Mg+Ca+Mn), *sps*(Grt) = Mn/(Fe^{2+}+Mg+Ca+Mn) for modelled isopleths.

Paragneiss of the Varied unit

On the macroscopic scale, paragneiss of the Varied unit has an opthalmitic to stromatitic texture. It is characterized by an alternation of biotite−rich melanosomes and leucocratic quartz−plagioclase−K-feldspar layers that define the steep S3 foliation as well as the subhorizontal S4 foliation. In thin section, the typical assemblage is seen to be Bt−Pl−Kfs−Qtz with abundant sillimanite and only rare garnet, muscovite and/or cordierite (Fig. 5-a,b). Small garnet grains (<1 mm in diameter) are preferentially present in the melanosome and locally contain muscovite and sillimanite inclusions. Garnet is commonly surrounded by plagioclase−K-feldspar coronas and by biotite−sillimanite aggregates oriented parallel to the S4 fabric (Fig. 5a). Accordingly, the isometric to elongated (up to 1 cm in length) biotite−sillimanite−K-feldspar−plagioclase nodules that are present in some samples are interpreted as pseudomorphs replacing former garnet porphyroblasts. Rare, randomly oriented muscovite is either large (up to 5 mm in size) or fine-grained. Pinitized cordierite (up to few millimeters in size) without shape-preferred orientation shows no pressure shadows and is interpreted as having grown after the D4 event (Fig. 5b). Rutile is included in garnet, and accessory ilmenite, graphite and pyrite are present in the matrix.

One sample of garnet-bearing paragneiss (BP12d) was selected for analysis of mineral chemistry. The sample contains the assemblage Grt−Sil−Bt−Pl−Kfs−Qtz−Ilm. An alternation of biotite-rich layers and elongated aggregates of quartz, plagioclase (*Ab* = 0.65−0.61, *An* = 0.34−0.38, *Or* = 0.01) and K-feldspar (*Ab* = 0.06−0.18, *An* = 0.01, *Or* = 0.81−0.93) defines the S4 foliation. Garnet (up to 1 mm in size) contains inclusions of sillimanite that are oriented at a high angle to the external S4 fabric in the core, but parallel to the external S4 fabric at the rim. Garnet is almandine-rich and shows a weak compositional zoning with slightly increasing spessartine and *X*Fe, and slightly decreasing pyrope and almandine from core (*Alm* = 0.73, *Prp* = 0.16, *Grs* = 0.03, *Sps* = 0.08, *X*Fe = 0.81) to rim (*Alm* = 0.72, *Prp* = 0.12, *Grs* = 0.04, *Sps* = 0.12, *X*Fe = 0.86). Garnet is surrounded by thin (< 50 μm) coronas of plagioclase−K-feldspar and thicker (up to 1 cm in length), elongated sillimanite−biotite aggregates developed in garnet pressure shadows generated during the D4 deformation. Biotite is preferentially oriented parallel to the S4 fabric; its composition shows *X*Fe = 0.56−0.60 and Ti = 0.15−0.20 a.p.f.u. Rare muscovite (up to few millimetres in size) does not show any preferential orientation and is interpreted as post-tectonic; it has Si = 3.04−3.10 a.p.f.u. and Na = 0.03−0.06 a.p.f.u..

Paragneiss of the Monotonous unit

Paragneiss of the Monotonous unit is opthalmitic to stromatitic with up to cm-scale quartzo-feldspathic augen or cm-scale leucosome layers alternating with biotite−sillimanite-rich layers (Fig. 5c). This alternation defines both the S3 and S4 fabrics. The most common assemblage is Sil−Bt−Pl−Kfs−Qtz with subordinate garnet, muscovite, cordierite and andalusite. Garnet porphyroblasts (up to 1 mm in diameter) include muscovite, biotite, K-feldspar and sillimanite. Plagioclase rarely contains small inclusions of garnet (~300 μm in size), kyanite (~100 μm in length), sillimanite or biotite (~100 μm), and micron-scale K-feldspar exsolution (Fig. 5c,d). Sillimanite−biotite intergrowths occur parallel to the S3 foliation, in the hinge zone of the F4 microfolds, and parallel to the S4 foliation. Muscovite (up to 3 mm in size) commonly includes sillimanite; it either lies parallel to the S3 and S4 foliations, or is randomly oriented (Fig. 5f). This is interpreted as a result of late growth that may occur parallel to the existing structures. Muscovite also occurs along cracks within garnet. Static cordierite porphyroblasts are observed in biotite-rich nests occurring in the S4 foliation (Fig. 5e). Therefore it is interpreted as a post-tectonic phase. Rutile is included in garnet while ilmenite occurs in the matrix. Chlorite locally replaces biotite and contains rutile needles.

Sample BP45a is an opthalmitic paragneiss preserving relicts of the S3 foliation in the hinge zone of the F4 microfolds. The relict S3 is defined by elongated leucocratic aggregates alternating with biotite−sillimanite-rich layers (Fig. 5c). In general, the S3 foliation is almost completely transposed into the S4 fabric. The sample contains an assemblage of Grt−Sil−Bt−Pl−Kfs−Qtz±Ky±Ms. Garnet (~0.5 mm in size) occurs in plagioclase (Fig. 5c) and includes plagioclase and K-feldspar. It shows no compositional

variation (*Alm* = 0.59−0.61, *Prp* = 0.17−0.19, *Grs* = 0.01−0.02, *Sps* = 0.18−0.20, *X*Fe = 0.76−0.78). Biotite is aligned in the S4 fabric; its composition shows *X*Fe = 0.48−0.51 and Ti = 0.12−0.16 a.p.f.u.. Plagioclase is chemically unzoned oligoclase (*Ab* = 0.81, *An* = 0.19, *Or* = 0.00) with lamellae of K-feldspar (few tens of microns in size, *Ab* = 0.04−0.05, *An* = 0.00, *Or* = 0.95−0.96) and contains rare inclusions of kyanite (Fig. 5d). Muscovite is rare, randomly oriented and commonly includes sillimanite aggregates, suggesting growth after the D4 deformation event (Fig. 5f); it has Si = 3.01−3.04 a.p.f.u. and Na = 0.03−0.08 a.p.f.u.. Ilmenite occurs in the matrix while rutile is present only as needles in chloritized biotite.

Micaschist and paragneiss of the Kaplice unit

In micaschist and paragneiss, the S3 foliation is characterized by an alternation of quartz-rich and mica-rich layers that are folded, and in places completely transposed into the S4 fabric (Fig. 6a). Numerous quartz segregations and rare leucosomes in paragneiss are also found parallel to the S3 and S4 foliations. The typical assemblage is Ms−Bt−Pl−Qtz in micaschist and Bt−Pl−Qtz in paragneiss. Sillimanite, rare garnet, and subordinate staurolite are locally observed in micaschist. Garnet is small (up to 1 mm in size), exhibits a clear core and a cloudy rim, and contains inclusions of rutile and ilmenite (Fig. 6b). The pressure shadows around garnet are related to the development of the S4 fabric and are dominated by partly chloritized biotite. Staurolite is elongated parallel to the S3 fabric (Fig. 6b). Sillimanite is mainly parallel to the S4 fabric, but is also present in the hinge zone of the F4 microfolds, indicating that it was already stable in the S3 foliation. In micaschist abundant muscovite is aligned parallel to both the S3 and S4 foliations (Fig. 6a), and is considered to be part of the primary metamorphic assemblage. Muscovite including rare sillimanite is regarded as a late overgrowth. Kyanite is rarely found around quartz segregations parallel to the S3 fabric, whereas oriented sillimanite is observed around quartz segregations parallel to the S4 fabric. Cordierite and andalusite are also found at the margins of quartz segregations that are elongated parallel to the S4 fabric (Fig. 6c,d); they probably developed at the end of D3 or after the D4 event. Matrix cordierite, which is not associated with quartz segregations, occurs only in samples collected from around the granite batholith in the southern part of the area. It does not show pressure shadows and is interpreted to have grown after the D4 event. Accessory minerals in the matrix are ilmenite, tourmaline and rutile. Rutile surrounding ilmenite is included in garnet. Rutile is also associated with chlorite that occurs around biotite and in the hinge zone of the F5 crenulation microfolds.

Sample BP64a chiefly preserves the macroscopic S4 foliation, but relicts of the S3 foliation are observed in thin section. The S3 relicts appear as microfolded quartz-rich aggregates oriented at a high angle to the S4 fabric. The rock contains an assemblage of Grt−St−Sil−Bt−Ms−Pl−Kfs−Qtz−Ilm±Tur. Garnet (1 mm in size) has pressure shadows associated with the development of the S4 foliation (Fig. 6b). It shows compositional zoning (Fig. 8c,d), with decreasing grossular, spessartine and *X*Fe, and increasing

almandine and pyrope from the core (*Alm* = 0.66, *Prp* = 0.04, *Grs* = 0.14, *Sps* = 0.16, *X*Fe = 0.95) to the inner rim (*Alm* = 0.78, *Prp* = 0.07, *Grs* = 0.07, *Sps* = 0.08, *X*Fe = 0.92). The ~100μm-large outermost rim shows an increase in spessartine balanced by a decrease in almandine (*Alm* = 0.74, *Prp* = 0.06, *Grs* = 0.05, *Sps* = 0.16, *X*Fe = 0.93). Rare staurolite (up to 0.8 mm in size) contains quartz inclusions trails that lie parallel to the S3 fabric, and is partly replaced by fine-grained muscovite and chlorite (Fig. 6b); its composition shows *X*Fe = 0.85−0.87. Muscovite parallel to both the S3 and S4 fabrics has Si = 3.04−3.07 a.p.f.u. and Na = 0.15−0.19 a.p.f.u. Biotite parallel to S3 or S4 has a similar *X*Fe = 0.64−0.68 and Ti = 0.07−0.11 a.p.f.u. Rare sillimanite is aligned parallel to the S4 foliation. K-feldspar is rare (*Ab* = 0.01, *An* = 0.01, *Or* = 0.98), and abundant plagioclase is of oligoclase composition (*Ab* = 0.09−0.11, *An* = 0.88−0.90, *Or* = 0.01). Ilmenite occurs in the matrix while rutile was not observed in this sample.

MINERAL EQUILIBRIA MODELLING

Calculation method

Pseudosections were calculated using THERMOCALC 3.3 (Powell *et al.*, 1998; 2009 version) and dataset 5.5 (Holland & Powell, 1998; November 2003 upgrade) in the system $MnO{-}Na_2O{-}CaO{-}K_2O{-}FeO{-}MgO{-}Al_2O_3{-}SiO_2{-}H_2O{-}TiO_2{-}O_2$ (MnNCKFMASHTO). Pseudosections were assembled using the TCWizard package (Petri & Skrzypek, 2013). Activity−composition relationships are after: White *et al.* (2005), for garnet, biotite and ilmenite; Mahar *et al.* (1997) and Holland & Powell (1998), for cordierite and staurolite; White *et al.* (2007), for granitic melt; Holland & Powell (2003), for feldspars; and, Coggon & Holland (2002), for white mica. Molar and compositional isopleths were plotted for the phases of interest, especially for modelling the garnet zoning at specific *P–T* conditions and/or along given *P–T* segments.

Pseudosections were calculated for whole rock compositions obtained by ICP−AES (Acme Laboratories, Canada); compositions are presented in Table 2. The proportion of Fe_2O_3 (O value) for modelling was set to 0.01 to reflect the generally reduced character of pelitic rocks. Moreover, this value allows both ilmenite and rutile to be stable in the modelled *P–T* domain.

For migmatitic paragneiss samples of the Varied and Monotonous units, mineral equilibria modelling follows an approach detailed by Hasalová *et al.* (2008b). It assumes that the last suprasolidus assemblage tends to continuously equilibrate until it becomes melt absent (Guiraud *et al.*, 2001; Powell *et al.*, 2005; Štípská & Powell, 2005). Therefore, the amount of H_2O is chosen after the construction of *T–M*(H_2O) sections so that (1) the solidus bounds the stability field of the matrix assemblage observed in thin section, and (2) garnet compositional isopleths lie close to the measured garnet composition. Because muscovite-rich micaschist of the Kaplice unit shows numerous quartz segregations and few to no leucosomes, it is suggested that H_2O was present rather

than granitic melt. Accordingly, the pseudosection is modelled with excess quartz and muscovite, and at H_2O-saturated conditions.

Varied unit: Pseudosection for paragneiss sample BP12d

Using H_2O = 4.26 mol.% for the whole rock composition of sample BP12d (Table 2) allows the observed assemblage Grt−Sil−Bt−Pl−Kfs−Qtz−Ilm−Liq with *alm*(Grt) = 0.75 to be stable close to the liquid-out line in the pseudosection (Fig. 9). A lower H_2O content would shift the solidus to higher temperatures, where the *alm*(Grt) and *sps*(Grt) isopleth values are too low compared to the measured garnet composition, whereas a higher H_2O content does not allow for garnet stability at the liquid-in line. The major features of the pseudosection involve the H_2O-undersaturated solidus between 3 kbar/650 °C and 12 kbar/800 °C, the muscovite-out line from 1 kbar/525 °C to 6 kbar/700 °C and to 12 kbar/800 °C. Biotite is not stable above 750−800 °C, garnet is not stable below 5 kbar and 700 °C, cordierite is stable above 550 °C and 1 kbar, and at pressures lower than 7 kbar for temperatures higher than 800 °C. The ilmenite−rutile transition occurs between 6 and 8 kbar.

Textural relationships in sample BP12d point to an initial garnet growth in equilibrium with sillimanite. In other samples, rutile is included in garnet indicating growth in the rutile stability field. Garnet preserves sillimanite inclusion trails perpendicular and parallel to the S4 foliation (Fig. 5a), suggesting that the garnet−sillimanite assemblage was stable during the D4 deformation, and possibly also during the D3 deformation. Garnet additionally shows a weak compositional zoning with only slightly increasing spessartine and *X*Fe, and decreasing pyrope and almandine at the rim (Fig. 8a). After the equilibration of the dominant matrix assemblage Grt−Sil−Bt−Pl−Kfs−Qtz−Ilm, the abundant occurrence of sillimanite and biotite around garnet and in the pressure shadows associated with D4 points to garnet breakdown during the D4 event. It is followed by a localized post-tectonic muscovite growth.

In the pseudosection, the textural features are compatible with an initial decompression path from the Grt−Sil−Bt−Pl−Kfs−Qtz−Rt−Liq to the Grt−Sil−Bt−Pl−Kfs−Qtz−Ilm−Liq field (Fig. 9a). Decompression should be accompanied by heating to allow an increase in garnet molar proportion in the sillimanite−rutile stability field (Fig. 9b). Further decompression and cooling in the Grt−Sil−Bt−Pl−Kfs−Qtz−Ilm−Liq field should occur to account for a decrease in garnet molar proportion simultaneous with an increase in sillimanite and biotite molar proportions. The nearly constant garnet core composition is interpreted as a result of diffusional equilibration that occurred at ~5.5 kbar and 750 °C, as indicated by the modelled compositional isopleths (Fig. 9b,c). The compositional variation at the garnet rim is compatible with a re-equilibration during cooling at ~4.5 kbar and 700 °C.

Monotonous unit: Pseudosection for paragneiss sample BP45a

Using H_2O = 3.38 mol.% for the whole rock composition of sample BP45a (Table 2) allows the observed assemblage Grt−Sil−Bt−Pl−Kfs−Qtz−Ilm−Liq with *alm*(Grt) = 0.64 to be stable close to the liquid-out line in the pseudosection (Fig. 10). A lower H_2O content would shift the solidus to higher temperatures and lower the *alm*(Grt) and *sps*(Grt) values along the solidus, whereas a higher H_2O content would shift the solidus to lower temperatures and increase the *alm*(Grt) and *sps*(Grt) values along the solidus. The major features of the pseudosection are very similar to those described in the pseudosection for the paragneiss sample from the Varied unit (Fig. 9).

Textural relationships in sample BP45a involve relicts of kyanite armoured in matrix plagioclase, and a matrix composed of sillimanite, biotite, plagioclase, K-feldspar, quartz, ilmenite and small garnet included in plagioclase. Kyanite is preserved as inclusion in large plagioclase grains occurring with quartz and anhedral garnet growing along Qtz−Pl grain boundaries. It is interpreted as an inclusion in suprasolidus plagioclase and indicates that the sample originally had the assemblage corresponding to the field Grt−Ky−Bt−Pl−Kfs−Qtz−Rt−Liq which is located above 8 kbar at 740−830 °C in the pseudosection (Fig. 10a). The occurrence of sillimanite in the matrix indicates a subsequent decompression to the Grt−Sil−Bt−Pl−Kfs−Qtz−Ilm−Liq(?) field. The constant garnet composition is interpreted as a result of diffusive equilibration that probably occurred during the pressure decrease at still elevated temperature conditions. Garnet isopleths point to $P-T$ conditions of 4.7 kbar and 700 °C for this stage, and support a re-equilibration in the sillimanite stability field at the solidus (Fig. 10b,c). The dominant matrix assemblage parallel to the S4 foliation is Sil−Bt−Pl−Kfs−Qtz−Ilm with rare garnet included in plagioclase. In the pseudosection, this assemblage occurs at subsolidus conditions between 4.5−6 kbar and 700 °C, where the molar proportion of garnet is less than 1 mol.%.

Kaplice unit: Pseudosection for micaschist sample BP64a

The pseudosection was calculated up to the conditions of partial melting (650–700 °C) with quartz, muscovite and H_2O in excess for the whole rock composition of sample BP64a (Table 2). The major features involve garnet stability above 520−550 °C and 2.5−4 kbar, chlorite stability up to 500–575 °C, staurolite stability from 540 °C (at 2.4 kbar) to 660 °C (at 7.5 kbar), and biotite stability over the whole range of calculated $P-T$ conditions (Fig. 11). The sillimanite-in line stretches from 4 kbar/570 °C to 6.2 kbar/650 °C, while andalusite is stable at pressures of 2.5−4 kbar for temperatures of 520−660 °C, and cordierite is stable at temperatures of 500−700 °C with an upper pressure limit at 3.5 kbar.

Crystallization−deformation relationships involve staurolite and quartz oriented parallel to the relict S3 foliation, garnet with pressure shadows formed due to the development of the S4 foliation, and muscovite, biotite and rare sillimanite aligned

parallel to the S4 fabric (Fig. 6a,b). Garnet shows decreasing grossular, spessartine and *X*Fe, and increasing almandine and pyrope from the core (*Alm* = 0.66, *Prp* = 0.04, *Grs* = 0.14, *Sps* = 0.16, *X*Fe = 0.95) to the inner rim (*Alm* = 0.78, *Prp* = 0.07, *Grs* = 0.07, *Sps* = 0.08, *X*Fe = 0.92). The outer rim composition (*Alm* = 0.74, *Prp* = 0.06, *Grs* = 0.05, *Sps* = 0.16, *X*Fe = 0.93) indicates an increase in spessartine balanced by a decrease in almandine mostly (Fig. 8c,d).

The sequence of crystallization points to a medium pressure prograde path followed by decompression (white arrow and circles 1 to 4 in Fig. 11). The beginning of the $P-T$ path is deduced from the garnet core composition that nearly matches the modelled isopleths at ~5.5 kbar and 520 °C along the garnet-in line (circle 1 in Fig. 11b,c). The occurrence of staurolite indicates further prograde evolution in the S3 fabric. This interpretation is supported by garnet zoning and the staurolite composition (*X*Fe = 0.86), for which the corresponding isopleths lie in the Grt−St−Ms−Bt−Pl−Qtz−Ilm−H_2O field at ~5.8 kbar/600 °C and 6.5 kbar/640 °C, respectively (circles 2 & 3 in Fig. 11b,c,d). The occurrence of kyanite around quartz segregations supports pressures higher than 6 kbar during the prograde path. Garnet composition points to slightly lower $P-T$ conditions. This discrepancy is explained by the slope of the garnet molar isopleths in the staurolite field, which suggests limited garnet growth along this part of the $P-T$ path. Alternatively, the garnet rim composition may have been modified during later re-equilibration. The presence of sillimanite indicates a progression into the sillimanite stability field, which occurred contemporaneously with the transition from the S3 to the S4 fabric. The absence of leucosome in the sample argues for a maximum temperature bounded by the liquid-in line at 650 °C. However, the maximum temperature could be slightly higher, because a small amount of melt would be difficult to recognize in thin section. Because rare leucosomes occur in the field, it is likely that the Kaplice unit reached conditions slightly above the solidus. The isopleths corresponding to the garnet outermost rim composition intersect in the Grt−Sil−Ms−Bt−Pl−Qtz−Ilm−H_2O field at 4.5 kbar and 660 °C, close to the limit of partial melting (circle 4 in Fig. 11b,c).

A theoretical garnet profile is calculated from the pseudosection isopleths (Fig. 8c). From the garnet-in line at 5.4 kbar and 530°C to 7.1 kbar and 660°C, garnet molar isopleths increase up to 3.5 mol.% (Fig. 11). The compositional variables at intervals of 0.25 mol.% of garnet are plotted on a profile where the garnet proportion is converted into a radius length assuming radial symmetry and a size equivalent to the analysed garnet. The similarity between the observed and modelled profiles suggests that garnet zoning reflects prograde growth (Fig. 8c).

The composition of garnet at 4.9 kbar and 647°C is plotted as the end-point of the modelled profile (Fig. 8c), i.e. where the isopleth *sps*(Grt) = 0.15 is crossed along the decompression and cooling part of the *P–T* path (Fig. 11). Diffusional modification was then allowed in the outermost rim of the modelled profile to try to reproduce the observed garnet zoning (Fig. 8c, see Appendix for details). Diffusion was modelled between the

end-point of the profile for a ~100µm penetration depth, which is deduced from the inflexion of the observed profile (point #8 of the modelled profile, equilibrated at 5.4 kbar/575°C). Diffused profiles were plotted for *Alm* and *Sps* (*Prp* and *Grs* values being too low to observe significant changes) using different time-spans of diffusion at 4.9 kbar/650°C. The measured profile is closely reproduced for durations not exceeding 1 Ma, whereas a strong homogenization of the profile is observed for longer durations.

^{40}Ar–^{39}Ar GEOCHRONOLOGY

Previous geochronology on rocks from the study area focused on the granulite massifs. To better document the thermal history of the region, we collected samples from the northern Blanský les granulite massif to the southern Kaplice unit along a profile perpendicular to the main lithological boundaries, with particular emphasis on samples showing the presence of the S3 or S4 foliation.

Analytical procedure

Single grains ^{40}Ar–^{39}Ar analyses of amphibole and biotite were performed by laser step-heating at Geoazur laboratory, Nice (see Appendix for detailed analytical procedure). Ages were calculated using the ArArCalc program (Koppers, 2002), the decay constants recommended by Steiger & Jäger (1977), the atmospheric ^{40}Ar/^{39}Ar ratio of 298.56 ± 0.1% (Lee *et al.*, 2006) and the probability of fit (*p*-value) compiled using Isoplot v. 3.75 (Ludwig, 2012). The criteria for defining plateau ages were as follows: (1) a plateau age should contain at least 70% of the total released ^{39}Ar, (2) there should be at least three successive steps in the plateau, (3) the probability of fit (*p*-value) of the integrated steps should be $p > 0.05$ (95% confidence level) and (4) the integrated age of the plateau should agree with each apparent age of the plateau within a 2σ error confidence interval.

^{40}Ar–^{39}Ar results

The ^{40}Ar–^{39}Ar step−release spectra are shown in Fig. 12. The full set of raw data is given as Supporting Information in Table S1. The location of all analysed samples is presented in Fig. 13.

Biotite 357 (experiment K511) [48.88641°N; 14.23274°E] was separated from a retrogressed felsic granulite from the Blanský les massif showing late crystallization of biotite. This biotite yields a disturbed age spectrum; we observe regularly decreasing ages with increasing laser heating (Fig. 12a). This disturbance is classically attributed to chlorite intercalations producing ^{39}Ar recoil from the biotite to the chlorite during the irradiation (Lo & Onstott, 1989; Ruffet *et al.*, 1991). The weighted age is 334 ± 5 Ma, which was calculated from 5 consecutive steps that together comprise 70% of the total ^{39}Ar released (MSWD = 1.07, $p = 0.37$). The isochron age is 340 ± 5. These ages must be interpreted with caution.

Amphibole 355 (experiment K510) [48.85230°N; 14.36436°E] was separated from an amphibolite sample from the Varied unit in the vicinity of the Blanský les massif.

Brown hornblende is aligned parallel to the S4 foliation, together with interstitial quartz, plagioclase and rare biotite. The plateau age of 339 ± 6 Ma (Fig. 12b) was obtained from 7 consecutive steps that together comprise 99.7% of the total ^{39}Ar released (MSWD = 1.36, p = 0.22).

Biotite 351 (experiment K514) [48.75512°N; 14.22660°E] was separated from an amphibolite sample from the Varied unit where rare euhedral biotite is in equilibrium with amphibole aligned parallel to the S4 fabric. The 300 ± 5 Ma "sub-plateau" age (Fig. 12c) was calculated from 5 steps that together comprise 69.6% of the total ^{39}Ar released (MSWD = 2.94, p = 0.038). As the p-value is below the cut-off value of 0.05, this age must be interpreted with caution.

Amphibole 351 (experiment K506) [48.75512°N; 14.22660°E] was separated from the same sample as *Biotite 351*. The amphibole is brown to brown-green hornblende forming aggregates elongated parallel to the S4 foliation. Quartz and plagioclase are interstitial. The plateau age of 341 ± 6 Ma (Fig. 12d) was calculated from 10 consecutive steps that together comprise 99.3% of the total ^{39}Ar released (MSWD = 1.11, p = 0.34).

Biotite 354 (experiment K508) [48.69249°N; 14.32622°E] was separated from a micaschist of the Kaplice unit. Muscovite and biotite alignment defines the S4 structure, with larger biotite crystals being systematically oblique to the S4 planar structure. Muscovite also forms fine-grained aggregates, probably after cordierite. A plateau age of 298 ± 4 Ma (Fig. 12e) was calculated from 6 consecutive steps that together comprise 84.0% of the total ^{39}Ar released (MSWD = 0.63, p = 0.68).

Biotite 360 (experiment K513) [48.79528°N; 14.40276°E] was separated from a micaschist of the Kaplice unit. Muscovite and biotite occur parallel to the S3 foliation, which is affected by F4 microfolds, with biotite and muscovite remaining stable in the hinge zone. Quartz forms leucocratic bands with plagioclase and shows high temperature grain boundary migration. The plateau age of 317 ± 4 Ma (Fig. 12f) was calculated from 11 consecutive steps that together comprise 87.4% of the total ^{39}Ar released (MSWD = 0.33, p = 0.97). The slightly staircase shape of the spectrum may suggest a reheating event younger than 280 Ma that does not appear to have affected the plateau age. In such a case, the 320 Ma age may represents either a crystallization age or a cooling age.

DISCUSSION

P−T−d evolution

Varied and Monotonous units

Samples from the Varied unit do not preserve any petrographic feature related to a prograde $P-T$ path associated with burial. In sample BP12d, the matrix assemblage Grt−Sil−Bt−Pl−Kfs−Qtz−Ilm and oriented sillimanite inclusions in garnet indicate garnet growth in the sillimanite stability field (Figs. 5a & 9a). Such a texture points to heating probably occurring during the transition from the S3 to S4 fabric. The occurrence of

rutile in other samples suggests that pressure may have exceeded ~7 kbar. The abundant biotite and sillimanite developed in the S4 pressure shadows around garnet indicate subsequent garnet replacement during cooling and decompression in the S4 fabric (Figs. 5a, 9a). The cooling path is deduced from garnet chemistry indicating diffusion at about 5.5 kbar and 750 °C, followed by later re-equilibration of the rim at about 4.5 kbar and 700 °C (Figs. 8a & 9a).

Samples from the Monotonous unit do not preserve prograde assemblages, leaving the $P-T$ path associated with burial unconstrained. In sample BP45a, peak metamorphic conditions are constrained by kyanite preserved as inclusion in a large plagioclase coexisting with coarse-grained quartz and tiny garnet developed along Qtz−Pl grain boundaries (Fig. 5d). It indicates the stability of the assemblage Grt−Ky−Bt−Pl−Kfs−Qtz−Rt, probably with a small amount of partial melt in the S3 fabric, at conditions above ~8 kbar at 740−830 °C. For sample BP45a, the matrix assemblage in the S4 foliation is Sil−Bt−Pl−Kfs−Qtz−Ilm with rare garnet included in plagioclase, which indicates garnet rim equilibration around 4.5−6 kbar and 700 °C. The constant compositional profile of small garnet grains is interpreted as resulting from diffusional re-equilibration that occurred around 4.5−5 kbar and 700 °C. If the Varied and Monotonous units contained garnet with an initial strong prograde zoning, as is commonly the case in metasedimentary rocks, the results for intracrystalline diffusion modelling from the Kaplice unit would suggest that garnets in the Varied and Monotonous units were probably homogenised by diffusion on the order of several Ma.

The presence of late cordierite in some samples of the Varied and Monotonous units indicates a $P-T$ path through the cordierite stability field after the D4 deformation. In the calculated pseudosections, cordierite stability lies very close to the end points of the inferred $P-T$ paths. Therefore, it is likely that for other bulk rock compositions, the cordierite stability field may extend up to the conditions of the end of the $P-T$ paths constrained using BP12d (Varied unit) and BP45a (Monotonous unit) samples. Alternatively, additional heating could have led to static growth of cordierite after the D4 deformation.

Kaplice unit

Samples from the Kaplice unit preserve several indicators that define a $P-T$ path. These are: the initial growth of staurolite parallel to the S3 fabric, garnet pressure shadows developed during the formation of S4, and biotite, muscovite and sillimanite affected by F4 microfolds (Fig. 6a,b). This sequence of crystallization points to a medium pressure prograde path, the beginning of which is recorded by the garnet core composition (circle 1 in Fig. 11b,c). Both staurolite composition and garnet zoning indicate a continuation of the prograde path up to 6.5 kbar and 640 °C (circles 2 & 3 in Fig. 11b,c,d). The textural characteristics of sillimanite indicate a progression towards the sillimanite stability field for both the S3 and S4 fabrics. Because no leucosomes are macroscopically observed, the

maximum temperature is limited by the liquid-in line at 650 °C, but may be slightly higher if a small amount of melt, which remains difficult to recognize, is actually present. The outermost rim of garnet is thought to record diffusional re-equilibration that occurred at 4.9 kbar and 650 °C (circle 4 in Fig. 11b,c) and lasted about 1 Ma (Fig. 8c,d).

Additional petrographic information from other samples is also correlated with the pseudosection to roughly estimate the *P–T* evolution during decompression, and to discuss possible variations in the *P−T* path for other parts of the Kaplice unit. The presence of rare leucosomes indicates that parts of the Kaplice unit underwent weak migmatization, with muscovite remaining stable. Considering that the upper stability of muscovite in the presence of quartz occurs at nearly constant *P−T* conditions for any felsic rock composition (see for example Figs. 9 & 10, e.g. Vielzeuf & Holloway, 1988), the maximum temperature conditions at 6−8 kbar should be about 700−740 °C. The maximum amount of melt that could be present at temperatures lower than the muscovite dehydration melting reaction is <5 mol.% (e.g. Vielzeuf & Schmidt, 2001; White *et al.*, 2001), which is consistent with the scarcity of macroscopic leucosomes in this unit. Late chlorite in the hinges of the F3 microfolds indicates cooling, probably associated with decompression, in most parts of the Kaplice unit. Matrix cordierite not associated with quartz segregations is only found around the granitic intrusions in the southern part of the area, and indicates pressures below 2−3 kbar at 530−700°C.

Geochronological constraints on the exhumation and cooling history

Using existing and new geochronological data, we constrain the cooling history of the granulites and the adjacent metasedimentary units, which involves three distinct stages (see Fig. 13 for references on existing ages). The first stage is documented by numerous U−Pb zircon ages and ^{40}Ar–^{39}Ar ages from amphibole and biotite that cluster in the interval 350−335 Ma. The second stage is defined by ^{40}Ar–^{39}Ar ages from biotite and muscovite that lie between 318 and 310 Ma. The third stage is recorded by younger ^{40}Ar–^{39}Ar biotite ages of *c*. 300 Ma, which are similar to the crystallization age of 301 ± 4 Ma (^{40}Ar–^{39}Ar plateau age on amphibole) reported for a dyke intruding the E part of the Kaplice unit (Vrána *et al.*, 2005).

U−Pb zircon ages of 350−340 Ma (Fig. 13a), which are characteristic for the HP granulites (Kröner *et al.*, 2000; Wendt *et al.*, 1994), are interpreted to reflect zircon crystallization from melt at the onset of cooling of the granulite (Roberts & Finger, 1997), as also proposed in the Variscan Vosges Mts. (Skrzypek *et al.*, 2012). Therefore, this age may correspond to the onset of the decompression and melting during the development of the S3 fabric (Franěk *et al.*, 2011a), as modelled by Lexa *et al.* (2011). The age of the subhorizontal S4 fabric is better constrained by the emplacement of syntectonic plutons during a horizontal spreading event at *c.* 340 Ma (Verner *et al.*, 2008; Žák *et al.*, 2005; 2012). The *c.* 337 Ma age of undeformed granitoids cross-cutting the subhorizontal S4 foliation provides an upper time limit for the D4 event (e.g. Janoušek & Gerdes, 2003). Our new ^{40}Ar–^{39}Ar amphibole and biotite ages from the Blanský les

granulite and the immediate vicinity indicate that cooling below ~500 °C and ~300 °C (closure temperatures of hornblende and biotite, respectively; Harrison, 1982; Harrison *et al.*, 1985) also occurred at 340–335 Ma in the study area (Fig. 13b,c). These age range is at least 10 Ma older than suggested in previous studies of this massif (Košler *et al.*, 1999; Svojtka *et al.*, 2002) or of other granulite massifs (e.g. the 323 ± 2 Ma Rb–Sr age for biotite in Saxony, Romer & Rötzler, 2001).

The second stage of the cooling history is documented by ^{40}Ar–^{39}Ar ages on micas of 319–310 Ma from the eastern margin of the Blanský les granulite and in the northern part of the metasedimentary units, representing cooling below ~400 °C to ~300 °C (closure temperature of muscovite and biotite, respectively; Harrison *et al.*, 2009 for muscovite; Fig. 13b,c). This group of ages is compatible with the geochronological record in the mostly post-tectonic granitoids of the South Bohemian plutonic complex. There, U−Pb zircon ages range from 338 to 315 Ma (e.g. Finger *et al.*, 1997), while ^{40}Ar–^{39}Ar and Rb–Sr ages lie between 328 and 320 Ma for the Eisgarn-type granite and 320 to *c.*310 Ma for the Weinsberg-type granite (Scharbert, 1998). Therefore, the 319–310 Ma ages from this study may be interpreted as a result of re-opening of the argon system related to the intrusion of post-tectonic granitoids. This hypothesis is supported by the *c.* 318 Ma U−Pb zircon age from a late muscovite-bearing granitic dyke crosscutting the eastern marginal part of the Blanský les granulite (Svojtka *et al.*, 2002).

Finally, the last stage occurs at *c.* 300 Ma, as documented by ^{40}Ar–^{39}Ar biotite ages restricted to the southern part of the study area. These ages are similar to the *c.* 300 Ma U−Pb monazite age from the Freistadt pluton (Friedl *et al.*, 1996; Gerdes *et al.*, 2003) and one ^{40}Ar–^{39}Ar amphibole plateau age of 301 ± 4 Ma from an associated dyke of quartz diorite (Vrána *et al.*, 2005). Consequently, we interpret these young biotite ages as reflecting re-opening of the argon system due to the thermal influence of the late Carboniferous Freistadt pluton and the associated granodioritic dyke swarm (Figs. 2,3,13b,c).

Thermo-mechanical evolution of the middle orogenic crust

Tectono-metamorphic significance of the subvertical fabric S3

In the less metamorphosed, mid-crustal Kaplice unit the vertical fabric S3 is associated with burial from ~5.4 kbar/530°C to 6.5 kbar/640°C (Fig. 15a). Conversely, the lower crustal granulite documents a synchronous exhumation from ~14–20 kbar/600–800°C to ~6–8 kbar/600–800°C (Franěk *et al.*, 2011b). The opposite $P-T$ trajectories indicate a vertical exchange of material during the D3 deformation. Important constraints on the nature of this vertical exchange process come from the $P-T$ record of the intermediate Varied and Monotonous units.

Regardless of the driving mechanism, the vertical exchange implies a twofold subdivision of the orogenic crust (e.g. Burg *et al.*, 2004). An antiformal domain is

defined by the region where only exhumation occurs; here, the deeper a material point is originally located, the more it will be exhumed (Fig. 15a). Conversely, the (rim) synformal domain only shows burial, which increases according to the original depth of a material point. Thus, the trajectory of any material point during D3 depends on its initial depth and its distance from the apical part of the rising lower crust (Warren & Ellis, 1996). The prograde $P-T$ record in the Kaplice unit points to an original position in a rim synform (Fig. 15a). On the other hand, the retrograde path inferred in the Monotonous unit suggests that it belonged to the antiformal domain (Fig. 15a). Finally, a burial or exhumation path can equally explain the peak $P-T$ conditions of the Varied unit, and its position relative to the antiformal and synformal domain remains uncertain.

Another approach to the relative position of the mid-crustal units is based on their relative temperature conditions. The temperature distribution during D3 will reflect two major processes. First, folding of the isotherms occurs during the genesis of the S3 fabric (e.g. Chamberlain, 1986). Second, exhumation of hot granulite (~800 °C) into the middle crust, advecting heat that will steepen the isotherms in the surrounding rocks (Fig. 15a), as shown by numerical models of rising diapirs (e.g. Gerya *et al.*, 2004). The Kaplice unit documents burial along a gradient of ~30°C/km (Fig. 11). These hot conditions point to a relative proximity to the granulite. The Varied and Monotonous units show higher temperatures of 725−775 °C, and a longer residence at such conditions is supported by homogenization of any prograde compositional zoning in garnet porphyroblasts (Figs. 8,10 & 11). Therefore, it is likely that both units were located close to the exhuming granulites during D3.

This discussion highlights that the rocks were not only juxtaposed at a similar depth, but likely occupied a similar horizontal position in relation to the granulites (Fig. 15a). Although rise of hot lower crustal material may be controlled by gravitational forces alone (e.g. Ramberg, 1981), the tight juxtaposition of mid-crustal rocks as well as the rate of exhumation suggests associated lateral shortening (Lexa *et al.*, 2011). Therefore, we suggest that the horizontal shortening associated with D3 likely assisted the vertical exchange of material. The genesis of antiformal and synformal domains, though overprinted by the D4 deformation, and the shape of the $P-T$ paths are ascribed to large-scale folding, as recognized previously in similar settings in the Bohemian Massif (Racek *et al*., 2006; Skrzypek *et al.*, 2011; Štípská *et al*., 2012).

Tectono-metamorphic significance of the subhorizontal fabric S4

In the mid- and lower crustal units, the subhorizontal S4 foliation is related to exhumation to a common depth of ~15−18 km (4.5−5.5 kbar, Fig. 15b). Three processes could have generated this juxtaposition of different crustal levels.

First, a similar subhorizontal foliation along the eastern margin of the Moldanubian domain is interpreted to be the result of channel flow (e.g. Štípská *et al.*, 2008). This model accounts for the isobaric heating from 650 to 750 °C (at 7 kbar),

which is documented in the Varied and Monotonous units (Racek *et al.*, 2006; Štípská *et al.*, 2008), and the *P*−*T* decrease from 7 kbar/790 °C to 4.5 kbar/690 °C documented in the Gföhl orthogneiss (Hasalová *et al.*, 2008a,b). In this study, all lithologies record a decrease in *P*−*T* conditions, from 7 kbar and 650−750 °C to 4.5 kbar and 660–700 °C (Figs. 14 & 15b; Verner *et al.*, 2008), which is inconsistent with the *P*−*T* evolution associated with channel flow.

Second, a similar *P*−*T*−*d* evolution to this study could be produced by extensional detachment faulting, a feature which is commonly observed in the European Variscan Belt (e.g. Rey, 1993; Brown & Dallmeyer, 1996; Vanderhaeghe & Teyssier, 2001). This extension is a consequence of a delamination of the lithospheric root (Rey et al., 2001) and associated gravitational collapse (e.g. Dewey *et al.*, 1993; Milnes & Koyi, 2000). However, in the European Variscan Belt, this process occurs about 10−20 Ma after crustal thickening, as illustrated by the Late Carboniferous age of most detachment zones (e.g. Burg *et al.*, 1994). In addition, no observations support an extensional origin for the S4 foliation in the study area.

Third, juxtaposition of units with contrasting *P*−*T* conditions and subhorizontal foliation may occur during ductile thinning (Feehan & Brandon, 1999; Ring & Brandon, 1999). Numerical modelling shows that during ductile thinning a zone of horizontal foliation may develop in a mid-crustal horizon that has been thermally weakened by exhuming granulites (Maierová *et al.*, 2014). According to Maierová *et al.* (2014), the thermal structure of this zone, called the infrastructure−superstructure transition zone (ISTZ), can account for the decreasing *P*−*T* conditions similar to those observed in the mid-crustal units of this study and in mid-crustal metasedimentary rocks of the NE Bohemian Massif (Skrzypek *et al.*, 2011). However, the granulites may conduct heat into the surrounding rocks during exhumation (e.g. Chopin *et al.*, 2012), which might explain the temperature difference between the Kaplice and the Varied and Monotonous units, and constrain the relative position of these units with respect to the granulites (Fig. 15b).

Thermochronological data indicate fast cooling of the whole domain during the late-stage of the D4 deformation (Fig. 13). ^{40}Ar–^{39}Ar amphibole ages in the Varied unit overlap U–Pb zircon ages from granulites affected by both S3 and S4 fabrics (Franěk *et al.*, 2011a; Kröner *et al.*, 2000). In addition, the oldest amphibole ages of 341 and 339 Ma and ^{40}Ar–^{39}Ar biotite age of 334 Ma constrain the cooling of the ISTZ in this area (Fig. 12a). However, elsewhere the ISTZ is thought to stay hot for a significantly longer period of up to 10 Ma (Maierová *et al.*, 2014; Chopin *et al.*, 2012), suggesting that the duration of HT conditions in the ISTZ is not uniform. The internal parts of an orogen may be rapidly cooled if the volume of exhuming lower crust is low or if the rocks are rapidly brought to shallower depth. After exhumation and cooling the middle crust may be affected by emplacement of late-orogenic plutons, which provide local, short-lived sources of heat to re-open the argon isotopic system in both micas and amphiboles (Fig. 15c).

Origin of the present-day structural and metamorphic pattern

Taking into account the succession of lithological units to the North of the Blanský les massif, we postulate that the original tectono-stratigraphy with increasing depth was Kaplice unit, Varied unit, Monotonous unit and the HP granulites (Fig. 15). To the SE of the massif, this layering is disrupted (Fig. 3), possibly during D3 deformation, since $P-T$ data suggest a significant thinning of the lithological units in the limbs of the large-scale asymmetrical F3 folds (Fig. 15a). However, in the NE Bohemian Massif rocks that are not affected by vertical shortening preserve an intermediate ~5 km thick orthogneiss layer (Štípská *et al*., 2012), whereas in areas affected by shortening the orthogneiss layer is <1 km thick (Skrzypek *et al*., 2011). This suggests that the D4 deformation has modified the original layering of the middle crust. Therefore, we postulate that it is the superposition of D4 on D3 that caused the present-day structural and metamorphic pattern. This pattern implies the existence of two major thrust boundaries, one located between the granulite and the Varied unit, and the other located between the Monotonous and the Kaplice units (Figs. 3 & 15). Since no kinematic indicators are observed along these contacts, they are interpreted as apparent thrusts that result from the superposition of fabrics rather than active thrusting.

The major S4 fabric is moderately dipping to the NW in a large area rimming the western part of the South Bohemian plutonic complex, but is almost subhorizontal or gently NW-dipping to the W of the granulite massifs (Franěk *et al.*, 2011a). The opposite structural pattern is recognized to the E of the South Bohemian plutonic complex where the S4 foliation is moderately to gently dipping to the E in the Monotonous unit close to the eastern margin of the pluton, but forms a subhorizontal bowl-like structure farther E (Fuchs, 1976). Therefore, we argue that the S4 foliation was originally sub-horizontal and the later perturbation is due to late Carboniferous extensional shearing (e.g. Burg *et al.*, 1994; Lobkowicz *et al.*, 1996), and diapiric upwelling of the central part of the South Bohemian plutonic complex, as proposed for its northern extension by Verner *et al.* (2014).

ACKNOWLEDGMENTS

B.P. acknowledges the University of Strasbourg for financial support. We acknowledge funding from the Ministry of Education of the Czech Republic (grant LK11202 to K.S.) and from the Czech National Grant Agency (grant no. 13−16315S to P.S.). E.S. acknowledges a Postdoctoral Fellowship from the Japan Society for the Promotion of Science (JSPS). The work of J.F. was supported by the GAČR Project P210-11-2358. Sylvain Gallet is thanked for the early processing of geochronological data. F. Jourdan, J. Žák and P. Pitra are thanked for their constructive reviews as well as M. Brown for his careful editorial work.

REFERENCES

Aftalion, M., Bowes, D. R. & Vrána, S., 1989. Early carboniferous U-Pb zircon age of garnetiferous, perpotassic Granulites, Blanský les massif, Czechoslovakia. *Neues Jahrbuch für Mineralogie*, **4**, 145-152.

Ahrendt, H., Clauer, N., Hunziker, J.C., Weber, K., 1983. Migration of folding and metamorphism in the Rheinisches Schiefergebirge deduced from K–Ar and Rb–Sr-age determinations. In: Martin, H., Eder, F.W. (Eds.), *Intracontinental Fold Belts. Springer Verlag*, Heidelberg, Berlin, pp. 323–338.

Beaumont, C., Jamieson, R. A., Nguyen, M. H. & Lee, B., 2001. Himalayan tectonics explained by extrusion of a low-viscosity crustal channel coupled to focused surface denudation. *Nature*, **414**, 738-742.

Brown, M. & Dallmeyer, R. D., 1996. Rapid Variscan exhumation and the role of magma in core complex formation: southern Brittany metamorphic belt, France. *Journal of Metamorphic Geology*, **14**, 361-379.

Burg, J.-P., Van Den Drissche, J. & Brun, J.-P., 1994. Syn- to post-thickening extension in the Variscan Belt of Western Europe: Modes and structural consequences. *Géologie de la France*, **3**, 33-51.

Burg, J.-P., Kaus, B. J. P. & Podladchikov, Y. Y., 2004. Dome structures in collision orogens: Mechanical investigation of the gravity/compression interplay. *Geological Society of America Special Papers*, **380**, 47-66.

Carswell, D. A. & O'Brien, P. J., 1993. Thermobarometry and Geotectonic Significance of High-Pressure Granulites: Examples from the Moldanubian Zone of the Bohemian Massif in Lower Austria. *Journal of Petrology*, **34**, 427-459.

Chakraborty, S. & Ganguly, J., 1992. Cation diffusion in aluminosilicate garnets: experimental determination in spessartine-almandine diffusion couples, evaluation of effective binary diffusion coefficients, and applications. *Contributions to Mineralogy and Petrology*, **111**, 74-86.

Chamberlain, C. P., 1986. Evidence for the Repeated Folding of Isotherms during Regional Metamorphism. *Journal of Petrology*, **27**, 63-89.

Chopin, F., Schulmann, K., Skrzypek, E., Lehmann, J., Dujardin, J.-R., Martelat, J.-E., Lexa, O., Corsini, M., Edel, J.-B., Štípská, P. & Pitra, P., 2012. Crustal influx, indentation, ductile thinning and gravity redistribution in a continental wedge: building a Moldanubian mantled gneiss dome with underthrust Saxothuringian material (European Variscan belt). *Tectonics*, **31**, TC1013.

Crank, J., 1975. *The Mathematics of diffusion*. Oxford University Press, Oxford.

Coggon, R. & Holland, T. J. B., 2002. Mixing properties of phengitic micas and revised garnet-phengite thermobarometers. *Journal of Metamorphic Geology*, **20**, 683-696.

Dewey, J. F., Ryan, P. D. & Andersen, T. B., 1993. Orogenic uplift and collapse, crustal thickness, fabrics and metamorphic phase changes: the role of eclogites. *Geological Society, London, Special Publications*, **76**, 325-343.

Drábek, M. & Stein, H., 2003. The age of formation of a marble in the Moldanubian Varied Group, Bohemian massif, Czech Republic using Re-Os dating of a molybdenite. In: *Proc. of the SGA meeting*, pp. 973-976, Athens.

Edel, J.-B., Schulmann, K. & Holub, F. V., 2003. Anticlockwise and cloxkwise rotations of the Eastern Variscides accomodated by dextral lithospheric wrenching: palaeomagnetic and structural evidence. *Journal of the Geological Society*, **102**, 209-218.

Faryad, S. W., Perraki, M. & Vrána, S., 2006. P-T evolution and reaction textures in retrogressed eclogites from Svetlik, the Moldanubian Zone (Czech Republic). *Mineralogy and Petrology*, **88**, 297-319.

Faryad, S. W., Nahodilová, R. & Dolejs, D., 2010. Incipient eclogite facies metamorphism in the Moldanubian granulites revealed by mineral inclusions in garnet. *Lithos*, **114**, 54-69.

Feehan, J. G. & Brandon, M. T., 1999. Contribution of ductile flow to exhumation of low-temperature, high-pressure metamorphic rocks: San Juan-Cascade nappes, NW Washington State. *Journal of Geophysical Research: Solid Earth*, **104**, 10883-10902.

Finger, F., Roberts, M. P., Haunschmid, B., Schermaier, A. & Steyrer, H. P., 1997. Variscan granitoids of central Europe: their typology, potential sources and tectonothermal relations. *Mineralogy and Petrology*, **61**, 67-96.

Franěk, J., Schulmann, K. & Lexa, O., 2006. Kinematic and rheological model of exhumation of high pressure granulites in the Variscan orogenic root: example of the Blanský les granulite, Bohemian Massif, Czech Republic. *Mineralogy and Petrology*, **86**, 253-276.

Franěk, J., Schulmann, K., Lexa, O., Tomek, C. & Edel, J.-B., 2011a. Model of syn-convergent extrusion of orogenic lower crust in the core of the Variscan belt: implications for exhumation of HP rocks in large hot orogens. *Journal of Metamorphic Geology*, **29**, 53-78.

Franěk, J., Schulmann, K., Lexa, O., Ulrich, S., Štípská, P., Haloda, J. & Týcová, P., 2011b. Origin of felsic granulite microstructure by heterogeneous decomposition of alkali feldspar and extreme weakening of orogenic lower crust during the Variscan orogeny. *Journal of Metamorphic Geology*, **29**, 103-130.

Franke, W., 2000. The mid-European segment of the Variscides: tectonostratigraphic units, terrane boundaries and plate tectonic evolution. *Geological Society, London, Special Publications*, **179**, 35-61.

Friedl, G., Von Quadt, A. & Finger, F., 1996. Timing der Intrusionstätigkeit im Südböhmischen Batholith. In: *In: Symposion, Tektonik-Strukturgeologie-*

Kristallingeologie, Salzburg, 10-15 April 1996, book of abstracts, pp. 127-130, Fakultas Universitätsverlag, Vienna.

Friedl, G., Finger, F., Paquette, J.-L., von Quadt, A., McNaughton, N. J. & Fletcher, I., 2004. Pre-Variscan geological events in the Austrian part of the Bohemian Massif deduced from U–Pb zircon ages. *International Journal of Earth Sciences*, **93**, 802-823.

Fuchs, G., 1976. Zur Entwicklung der Böhmischen Masse. *Jahrbuch der Geologischen Bundesanstalt*, **119**, 45-61.

Ganguly, J., 2010. Cation diffusion kinetics in aluminosilicate garnets and geological applications. *Reviews in Mineralogy and Geochemistry*, **72**, 559-601.

Gerdes, A., Wörner, G. & Henk, A., 2000. Post-collisional granite generation and HT-LP metamorphism by radiogenic heating: the Variscan South Bohemian Batholith. *Journal of the Geological Society*, **157**, 577-587.

Gerdes, A., Friedl, G., Parrish, R. R. & Finger, F., 2003. High-resolution geochronology of Variscan granite emplacement the South Bohemian Batholith. *Journal of the Czech Geological Society*, **48**, 53-54.

Gerya, T. V., Perchuk, L. L., Maresch, W. V. & Willner, A. P., 2004. Inherent gravitational instability of hot continental crust: Implications for doming and diapirism in granulite facies terrains. *Geological Society of America Special Papers*, **380**, 97-115.

Guiraud, M., Powell, R. & Rebay, G., 2001. H_2O in metamorphism and unexpected behaviour in the preservation of metamorphic mineral assemblages. *Journal of Metamorphic Geology*, **19**, 445-454.

Grujic, D., Warren, C. J. & Wooden, J. L., 2011. Rapid synconvergent exhumation of Miocene-aged lower orogenic crust in the eastern Himalaya. *Lithosphere*, **3**, 346-366.

Harrison, T. M., 1982. Diffusion of 40Ar in hornblende. *Contributions to Mineralogy and Petrology*, **78**, 324-331.

Harrison, T. M., Duncan, I. & McDougall, I., 1985. Diffusion of 40Ar in biotite: Temperature, pressure and compositional effects. *Geochimica et Cosmochimica Acta*, **49**, 2461-2468.

Harrison, T. M., Célérier, J., Aikman, A. B., Hermann, J. & Heizler, M. T., 2009. Diffusion of 40Ar in muscovite. *Geochimica et Cosmochimica Acta*, **73**, 1039-1051.

Hasalová, P., Schulmann, K., Lexa, O., Štípská, P., Hrouda, F., Ulrich, S., Haloda, J. & Tycova, P., 2008a. Origin of migmatites by deformation-enhanced melt infiltration of orthogneiss: a new model based on quantitative microstructural analysis. *Journal of Metamorphic Geology*, **26**, 29-53.

Hasalová, P., Štípská, P., Powell, R., Schulmann, K., Janoušek, V. & Lexa, O., 2008b. Transforming mylonitic metagranite by open-system interactions during melt flow. *Journal of Metamorphic Geology*, **26**, 55-80.

Holland, T. J. B. & Powell, R., 1998. An internally consistent thermodynamic data set for phases of petrological interest. *Journal of Metamorphic Geology*, **16**, 309-343.

Holland, T. & Powell, R., 2003. Activity–composition relations for phases in petrological calculations: an asymmetric multicomponent formulation. *Contributions to Mineralogy and Petrology*, **145**, 492-501.

Janoušek, V. & Gerdes, A., 2003. Timing the mamatic activity within the Central Bohemian Pluton, Czech Republic: conventional U-Pb ages for the Sazáva and Tábor intrusions and their geotectonic significance. *Journal of the Czech Geological Society*, **48**, 70-71.

Janoušek, V., Finger, F., Roberts, M. P., Frýda, J., Pin, C. & Dolejš, D., 2004. Deciphering petrogenesis of deeply buried granites: whole-rock geochemical constraints on the origin of largely undepleted felsic granulites from the Moldanubian Zone of the Bohemian Massif. *Transactions of the Royal Society of Edinburgh: Earth Sciences*, **95**, 141-159.

Janoušek, V., Vrána, S., Erban, V., Vokurka, K. & Drábek, M., 2008. Metabasic rocks in the Varied Group of the Moldanubian Zone, southern Bohemia–their petrology, geochemical character and possible petrogenesis. *Journal of Geosciences*, **53**, 31-46.

Jourdan, F., Verati, C. & Féraud, G., 2006. Intercalibration of the Hb3gr 40Ar/39Ar dating standard. *Chemical Geology*, **231**, 177-189.

Klepeis, K. A., Clarke, G. L., Gehrels, G. & Vervoort, J., 2004. Processes controlling vertical coupling and decoupling between the upper and lower crust of orogens: results from Fiordland, New Zealand. *Journal of Structural Geology*, **26**, 765-791.

Konopásek, J. & Schulmann, K., 2005. Contrasting Early Carboniferous field geotherms: evidence for accretion of a thickened orogenic root and subducted Saxothuringian crust (Central European Variscides). *Journal of the Geological Society*, **162**, 463-470.

Koppers, A. A. P., 2002. ArArCALC--software for 40Ar/39Ar age calculations. *Computers & Geosciences*, **28**, 605-619.

Košler, J., Aftalion, M. & Bowes, D. R., 1993. Mid-late Devonian plutonic activity in the Bohemian Massif: U–Pb zircon isotopic evidence from the Staré Sedlo and Mirotice gneiss complexes, Czech Republic. *Neues Jahrbuch für Mineralogie, Monatshefte*, **1993**, 417-431.

Košler, J., Kelley, S. P., Vance, D. & Svojtka, M., 1999. Independent dating of cooling and decompression of high grade rocks in the southern Bohemian Massif with Ar-Ar, Sm-Nd and U-Pb techniques. In: *J. Conf. Abstracts*, pp. 39.

Košler, J., Konopásek, J., Sláma, J. & Vrána, S., 2014. U–Pb zircon provenance of Moldanubian metasediments in the Bohemian Massif. *Journal of the Geological Society*, **171**, 83-95.

Kotková, J., 1993. Tectonometamorphic history of lower crust in the Bohemian Massif: example of north Bohemian granulites. *Czech Geological Survey Special Paper*, 1-42.

Kotková, J., Kröner, A., Todt, W. & Fiala, J., 1996. Zircon dating of North Bohemian granulites, Czech Republic: further evidence for the Lower Carboniferous high-pressure event in the Bohemian Massif. *Geologische Rundschau*, **85**, 154-161.

Kotková, J., Schaltegger, U. & Leichmann, J., 2010. Two types of ultrapotassic plutonic rocks in the Bohemian Massif − Coeval intrusions at different crustal levels. *Lithos*, **115**, 163-176.

Kröner, A. & Willner, A. P., 1998. Time of formation and peak of Variscan HP-HT metamorphism of quartz-feldspar rocks in the central Erzgebirge, Saxony, Germany. *Contributions to Mineralogy and Petrology*, **132**, 1-20.

Kröner, A., O'Brien, P. J., Nemchin, A. A. & Pidgeon, R. T., 2000. Zircon ages for high pressure granulites from South Bohemia, Czech Republic, and their connection to Carboniferous high temperature processes. *Contributions to Mineralogy and Petrology*, **138**, 127-142.

Lee, J.-Y., Marti, K., Severinghaus, J. P., Kawamura, K., Yoo, H.-S., Lee, J. B. & Kim, J. S., 2006. A redetermination of the isotopic abundances of atmospheric Ar. *Geochimica et Cosmochimica Acta*, **70**, 4507-4512.

Lexa, O., Schulmann, K., Janoušek, V., Štípská, P., Guy, A. & Racek, M., 2011. Heat sources and trigger mechanisms of exhumation of HP granulites in Variscan orogenic root. *Journal of Metamorphic Geology*, **29**, 79-102.

Lo, C.-H. & Onstott, T. C., 1989. 39Ar recoil artifacts in chloritized biotite. *Geochimica et Cosmochimica Acta*, **53**, 2697-2711.

Lobkowicz, M., Štědrá, V. & Schulmann, K., 1996. Late-Variscan Extensional collapse of the thickened Moldanubian crust in South Bohemia. *Journal of the Czech Geological Society*, **41**, 123-138.

Ludwig, K.R., 2012. Isoplot v. 3.75: A geochronological toolkit for Microsoft Excel. Berkeley Geochronology Center, Special Publication No. 5, 75 pp.

Mahar, E. M., Baker, J. M., Powell, R., Holland, T. J. B. & Howell, N., 1997. The effect of Mn on mineral stability in metapelites. *Journal of Metamorphic Geology*, **15**, 223-238.

Maierová, P., Lexa, O., Schulmann, K. & Štípská, P., 2014. Contrasting tectono-metamorphic evolution of orogenic lower crust in the Bohemian Massif: A numerical model. *Gondwana Research*, **25**, 509-521.

Medaris, L. G., Fournelle, J. H., Ghent, E. D., Jelínek, E. & Mísař, Z., 1998. Prograde eclogite in the Gföhl Nappe, Czech Republic: new evidence on Variscan high-pressure metamorphism. *Journal of Metamorphic Geology*, **16**, 563-576.

Medaris, L. G., Beard, B. L. & Jelínek, E., 2006. Mantle-Derived, UHP Garnet Pyroxenite and Eclogite in the Moldanubian Gföhl Nappe, Bohemian Massif: A Geochemical Review, New P-T Determinations, and Tectonic Interpretation. *International Geology Review*, **48**, 765-777.

Milnes, A. G. & Koyi, H. A., 2000. Ductile rebound of an orogenic root: case study and numerical model of gravity tectonics in the Western Gneiss Complex, Caledonides, southern Norway. *Terra Nova*, **12**, 1-7.

Nahodilová, R., Štípská, P., Powell, R., Košler, J. & Racek, M., 2014. High-Ti muscovite as a prograde relict in high pressure granulites with metamorphic Devonian zircon ages (Běstvina granulite body, Bohemian Massif): Consequences for the relamination model of subducted crust. *Gondwana Research*, **25**, 630-648.

Nelson, K. D., Zhao, W., Brown, L. D., Kuo, J., Che, J., Liu, X., Klemperer, S. L., Makovsky, Y., Meissner, R., Mechie, J., Kind, R., Wenzel, F., Ni, J., Nabelek, J., Leshou, C., Tan, H., Wei, W., Jones, A. G., Booker, J., Unsworth, M., Kidd, W. S. F., Hauck, M., Alsdorf, D., Ross, A., Cogan, M., Wu, C., Sandvol, E. & Edwards, M., 1996. Partially Molten Middle Crust Beneath Southern Tibet: Synthesis of Project INDEPTH Results. *Science*, **274**, 1684-1688.

O'Brien, P. J. & Vrána, S., 1995. Eclogites with a short-lived granulite facies overprint in the Moldanubian Zone, Czech Republic: petrology, geochemistry and diffusion modelling of garnet zoning. *Geologische Rundschau*, **84**, 473-488.

Patočka, F., Kachlik, V., Dostal, J. & Frana, J., 2003. Granitoid gneisses with relict orbicular metagranitoids from the Varied Group of the southern Bohemian Massif Moldanubicum: Protolith derived from melting of Archaean crust? *Journal of the Czech Geological Society*, **48**, 100-101.

Petrakakis, K., 1997. Evolution of Moldanubian rocks in Austria: review and synthesis. *Journal of Metamorphic Geology*, **15**, 203-222.

Petri, B. & Skrzypek, E., 2013. TCWizard Matlab® package – Help File, 26/04/2013 update. Online report, University of Strasbourg. http://eost.unistra.fr/fileadmin/upload/EOST/Benoit_Petri/software1/TCWizard_HelpFile.pdf

Pitra, P. & Guiraud, M., 1996. Probable anticlockwise P,–T evolution in extending crust: Hlinsko region, Bohemian Massif. *Journal of Metamorphic Geology*, **14**, 49-60.

Powell, R., Holland, T. & Worley, B., 1998. Calculating phase diagrams involving solid solutions via non-linear equations, with examples using THERMOCALC. *Journal of Metamorphic Geology*, **16**, 577-588.

Powell, R., Guiraud, M. & White, R. W., 2005. Truth and beauty in metamorphic phase-equilibria: conjugate variables and phase diagrams. *The Canadian Mineralogist*, **43**, 21-33.

Racek, M., Štípská, P., Pitra, P., Schulmann, K. & Lexa, O., 2006. Metamorphic record of burial and exhumation of orogenic lower and middle crust: a new tectonothermal model for the Drosendorf window (Bohemian Massif, Austria). *Mineralogy and Petrology*, **86**, 221-251.

Ramberg, H., 1981. *Gravity, deformation and the earth's crust, in theory, experiments and geological application*. Academic Press, London.

Rey, P., 1993. Seismic and tectono-metamorphic characters of the lower continental crust in Phanerozoic areas: A consequence of post-thickening extension. *Tectonics*, **12**, 580-590.

Rey, P., Vanderhaeghe, O. & Teyssier, C., 2001. Gravitational collapse of the continental crust: definition, regimes and modes. *Tectonophysics*, **342**, 435-449.

Ring, U. & Brandon, M. T., 1999. Ductile deformation and mass loss in the Franciscan Subduction Complex: implications for exhumation processes in accretionary wedges. *Geological Society, London, Special Publications*, **154**, 55-86.

Roberts, M. P. & Finger, F., 1997. Do U-Pb zircon ages from granulites reflect peak metamorphic conditions? *Geology*, **25**, 319-322.

Romer, R. L. & Rötzler, J., 2001. P–T–t Evolution of Ultrahigh-Temperature Granulites from the Saxon Granulite Massif, Germany. Part II: Geochronology. *Journal of Petrology*, **42**, 2015-2032.

Ruffet, G., Féraud, G. & Amouric, M., 1991. Comparison of 40Ar-39Ar conventional and laser dating of biotites from the North Trégor Batholith. *Geochimica et Cosmochimica Acta*, **55**, 1675-1688.

Scharbert, S., 1998. Some geochronological data from the South Bohemian Pluton in Austria: a critical review. *Acta Universitatis Carolinae, Geologica, Praha*, **42**, 441-442.

Scheuvens, D., 2002. Metamorphism and microstructures along a high temperature metamorphic field gradient: the north–eastern boundary of the Královský hvozd unit (Bohemian Massif, Czech Republic). *Journal of Metamorphic Geology*, **20**, 413-428.

Schulmann, K., Kröner, A., Hegner, E., Wendt, I., Konopásek, J., Lexa, O. & Štípská, P., 2005. Chronological constraints on the pre-orogenic history, burial and exhumation of deep-seated rocks along the eastern margin of the Variscan orogen, Bohemian Massif, Czech Republic. *American Journal of Science*, **305**, 407-448.

Schulmann, K., Martelat, J.-E., Ulrich, S., Lexa, O., Štípská, P. & Becker, J. K., 2008. Evolution of microstructure and melt topology in partially molten granitic mylonite: Implications for rheology of felsic middle crust. *Journal of Geophysical Research*, **113**.

Schulmann, K., Konopásek, J., Janoušek, V., Lexa, O., Lardeaux, J.-M., Edel, J.-B., Štípská, P. & Ulrich, S., 2009. An Andean type Palaeozoic convergence in the Bohemian Massif. *Comptes Rendus Géoscience*, **341**, 266-286.

Siivola, J. & Schmid, R., 2007. Recommendations by the IUGS Subcommission on the Systematics of Metamorphic Rocks: List of mineral abbreviations. Web version 01.02.07. http://www.bgs.ac.uk/scmr/home.html

Skrzypek, E., Štípská, P., Schulmann, K., Lexa, O. & Lexová, M., 2011. Prograde and retrograde metamorphic fabrics – a key for understanding burial and exhumation in orogens (Bohemian Massif). *Journal of Metamorphic Geology*, **29**, 451-472.

Skrzypek, E., Štípská, P. & Cocherie, A., 2012. The origin of zircon and the significance of U–Pb ages in high-grade metamorphic rocks: a case study from the Variscan orogenic root (Vosges Mountains, NE France). *Contributions to Mineralogy and Petrology*, **164**, 935-957.

Sláma, J., Košler, J. & Pedersen, R. B., 2007. Behaviour of zircon in high-grade metamorphic rocks: evidence from Hf isotopes, trace elements and textural studies. *Contributions to Mineralogy and Petrology*, **154**, 335-356.

Steiger, R. J. & Jäger, E., 1977. Subcommission on geochronology: Convention on the use of decay constants in geo- and cosmochronology. *Earth and Planetary Science Letters*, **36**, 359-362.

Štípská, P., Schulmann, K. & Kröner, A., 2004. Vertical extrusion and middle crustal spreading of omphacite granulite: a model of syn-convergent exhumation (Bohemian Massif, Czech Republic). *Journal of Metamorphic Geology*, **22**, 179-198.

Štípská, P. & Powell, R., 2005. Does ternary feldspar constrain the metamorphic conditions of high-grade meta-igneous rocks? Evidence from orthopyroxene granulites, Bohemian Massif. *Journal of Metamorphic Geology*, **23**, 627-647.

Štípská, P., Schulmann, K. & Powell, R., 2008. Contrasting metamorphic histories of lenses of high-pressure rocks and host migmatites with a flat orogenic fabric (Bohemian Massif, Czech Republic): a result of tectonic mixing within horizontal crustal flow? *Journal of Metamorphic Geology*, **26**, 623-646.

Štípská, P., Powell, R., White, R. W. & Baldwin, J. A., 2010. Using calculated chemical potential relationships to account for coronas around kyanite: an example from the Bohemian Massif. *Journal of Metamorphic Geology*, **28**, 97-116.

Štípská, P., Chopin, F., Skrzypek, E., Schulmann, K., Pitra, P., Lexa, O., Martelat, J. E., Bollinger, C. & Žáčková, E., 2012. The juxtaposition of eclogite and mid-crustal rocks in the Orlica–Śnieżnik Dome, Bohemian Massif. *Journal of Metamorphic Geology*, **30**, 213-234.

Svojtka, M., 2001. *Geochronology and structural evolution of granulites in the southern Moldanubian Zone, Bohemian massif*. Thesis, Charles University, Prague.

Svojtka, M., Košler, J. & Venera, Z., 2002. Dating granulite-facies structures and the exhumation of lower crust in the Moldanubian Zone of the Bohemian Massif. *International Journal of Earth Sciences*, **91**, 373-385.

Tajčmanová, L., Konopásek, J. & Schulmann, K., 2006. Thermal evolution of the orogenic lower crust during exhumation within a thickened Moldanubian root of the Variscan belt of Central Europe. *Journal of Metamorphic Geology*, **24**, 119-134.

Timmermann, H., Dörr, W., Krenn, E., Finger, F. & Zulauf, G., 2006. Conventional and in situ geochronology of the Teplá Crystalline unit, Bohemian Massif: implications for the processes involving monazite formation. *International Journal of Earth Sciences*, **95**, 629-647.

Tollmann, A., 1982. Großräumiger Variszischer Deckenbau im Moldanubikum und Neue Gedanken zum Variszikum Europas. *Geotektonische Forschungen*, **64**.

Tropper, P., Deibl, I., Finger, F. & Kaindl, R., 2006. P–T–t evolution of spinel–cordierite–garnet gneisses from the Sauwald Zone (Southern Bohemian Massif, Upper Austria): is there evidence for two independent late-Variscan low-P/high-T events in the Moldanubian Unit? *International Journal of Earth Sciences*, **95**, 1019-1037.

Vanderhaeghe, O. & Teyssier, C., 2001. Partial melting and flow of orogens. *Tectonophysics*, **342**, 451-472.

Verner, K., Žák, J., Nahodilová, R. & Holub, F., 2008. Magmatic fabrics and emplacement of the cone-sheet-bearing Knížecí Stolec durbachitic pluton (Moldanubian Unit, Bohemian Massif): implications for mid-crustal reworking of granulitic lower crust in the Central European Variscides. *International Journal of Earth Sciences*, **97**, 19-33.

Verner, K., Žák, J., Šrámek, J., Paclíková, J., Zavřelová, A., Machek, M., Finger, F. & Johnson, K., 2014. Formation of elongated granite–migmatite domes as isostatic accommodation structures in collisional orogens. *Journal of Geodynamics*, **73**, 100-117.

Vielzeuf, D. & Holloway, J., 1988. Experimental determination of the fluid-absent melting relations in the pelitic system. *Contributions to Mineralogy and Petrology*, **98**, 257-276.

Vielzeuf, D. & Schmidt, M.W., 2001. Melting relations in hydrous systems revisited: application to metapelites, metagreywackes and metabasalts. *Contributions to Mineralogy and Petrology*, **141**, 251-267.

Vrána, S., 1979. Polyphase shear folding and thrusting in the Moldanubicum of southern Bohemia. *Bull. Geol. Surv. Prague*, **54**, 75-86.

Vrána, S. & Bártek, J., 2005. Retrograde metamorphism in a regional shear zone and related chemical changes: The Kaplice Unit of muscovite-biotite gneisses in the

Moldanubian Zone of southern Bohemia, Czech Republic. *Journal of the Czech Geological Society*, **50**, 43-57.

Vrána, S., Slaby, J. & Bendl, J., 2005. The Kaplice dyke swarm of biotite granodiorite porphyry and its relationship to the Freistadt granodiorite, Moldanubian Batholith. *Journal of the Czech Geological Society*, **50**, 9-17.

Warren, R. G. & Ellis, D. J., 1996. Mantle underplating, granite tectonics, and metamorphic P-T-t paths. *Geology*, **24**, 663-666.

Wegmann, C. E., 1935. Zur Deutung der Migmatite. *Geologische Rundschau*, **26**, 305-350.

Wendt, J., 1989. *U-Pb Zirkondatierung und Sm-Nd Systematik sowie Petrologie une Geochemie an Granuliten und Gneisen aus den Moldanubicum Südböhmens (ČSSR)*, Univerität Mainz.

Wendt, J., Kröner, A., Fiala, J. & Todt, W., 1993. Evidence from zircon dating for existence of approximately 2.1 Ga old crystalline basement in southern Bohemia, Czech Republic. *Geologische Rundschau*, **82**, 42-50.

Wendt, J., Kröner, A., Fiala, J. & Todt, W., 1994. U-Pb zircon and Sm-Nd dating of Moldanubian HP/HT granulites from South Bohemia, Czech Republic. *Journal of the Geological Society*, **151**, 83-90.

White, R. W., Powell, R. & Holland, T. J. B., 2001. Calculation of partial melting equilibria in the system Na2O–CaO–K2O–FeO–MgO–Al2O3–SiO2–H2O (NCKFMASH). *Journal of Metamorphic Geology*, **19**, 139-153.White, R. W., Pomroy, N. E. & Powell, R., 2005. An in situ metatexite–diatexite transition in upper amphibolite facies rocks from Broken Hill, Australia. *Journal of Metamorphic Geology*, **23**, 579-602.

White, R. W., Powell, R. & Holland, T. J. B., 2007. Progress relating to calculation of partial melting equilibria for metapelites. *Journal of Metamorphic Geology*, **25**, 511-527.

Willner, A. P., Rötzler, K. & Maresch, W. V., 1997. Pressure-Temperature and Fluid Evolution of Quartzo-Feldspathic Metamorphic Rocks with a Relic High-Pressure, Granulite-Facies History from the Central Erzgebirge (Saxony, Germany). *Journal of Petrology*, **38**, 307-336.

Žák, J., Holub, F. & Verner, K., 2005. Tectonic evolution of a continental magmatic arc from transpression in the upper crust to exhumation of mid-crustal orogenic root recorded by episodically emplaced plutons: the Central Bohemian Plutonic Complex (Bohemian Massif). *International Journal of Earth Sciences*, **94**, 385-400.

Žák, J., Verner, K., Holub, F. V., Kabele, P., Chlupáčová, M. & Halodová, P., 2012. Magmatic to solid state fabrics in syntectonic granitoids recording early Carboniferous orogenic collapse in the Bohemian Massif. *Journal of Structural Geology*, **36**, 27-42.

Zulauf, G., Dörr, W., Fiala, J. & Vejnar, Z., 1997. Late Cadomian crustal tilting and Cambrian transtension in the Teplá–Barrandian unit (Bohemian Massif, Central European Variscides). *Geologische Rundschau*, **86**, 571-584.

SUPPORTING INFORMATION

Additional Supporting Information may be found in the online version of this article:
Table S1. 40Ar−39Ar geochronology data.
Please note: Wiley-Blackwell are not responsible for the content or functionality of any supporting materials supplied by the authors. Any queries (other than missing material) should be directed to the corresponding author for the article.

APPENDIX

Mineral compositions analytical procedure

Mineral analyses were carried out at the University of Strasbourg on a TESCAN VEGA II XMU electron microscope and at the Charles University in Prague on a TESCAN VEGA III XM electron microscope, both equipped with EDS detectors. Operating conditions were 15 kV and 10 nA in Strasbourg, and 15kV and 1 nA in Prague.

^{40}Ar–^{39}Ar analytical procedure

Biotite and amphibole separates used for the experiments were obtained after sample crushing and handpicking single grains ranging from 0.5 to 1 mm in size under a binocular microscope. The minerals were repeatedly cleaned ultrasonically in distilled water. The carefully selected crystals were co-irradiated for 30 h in the nuclear reactor at the McMaster University in Hamilton (Canada), in position 5c, along with Hb3gr amphibole standard (1073.6 ± 5.4 Ma, Jourdan *et al.*, 2006). The total neutron flux density during irradiation was 8.8E18 n.cm^{-2} with a maximum flux gradient estimated at 0.2 % in the volume where the samples were included. ^{40}Ar–^{39}Ar analyses were performed at Geoazur laboratory, Nice. Single grains of amphibole and biotite were heated with a CO_2 Synrad laser, and the extracted gas was purified in a stainless and glass extraction line using two Al–Zr getters (working at 400 °C and ambient temperature, respectively) and a liquid nitrogen cold trap. Isotopic measurements were performed with a VG3600 mass spectrometer and a Daly−photomultiplier system. Blank measurements were obtained before and after every three samples run.

Diffusion modelling

Curves presented in Fig. 8.c were obtained using the equation of diffusion in an infinite sheet with a source of constant composition given by Eq. 1 (Crank, 1975).

$$C_{(x,t)} = C_1 + (C_0 - C_1)\mathrm{erf}\left(\frac{x}{2\sqrt{Dt}}\right) \quad (1)$$

where C_0 is the core concentration (mol.%), C_1 the rim concentration (mol.%), x the penetration depth (cm), D the diffusion coefficient (cm^2/s), and t time (s). D coefficients were determined at 4.9 kbar and 650°C for each element using Eq. 2 (Ganguly, 2010) and the parameters of Chakraborty & Ganguly (1992).

$$D_{(P,T)} = D_0 + e^{\left(\frac{-Q_{1\ bar} - (P-1)\Delta V^+}{RT}\right)} \qquad (2)$$

where $Q_{1\ bar}$ is the activation energy at 1 bar (J/mol), P pressure (bar), ΔV^+ the activation volume of diffusion (cm^3/mol), R the gaz constant (J/mol/K) and T temperature (K).

FIGURES

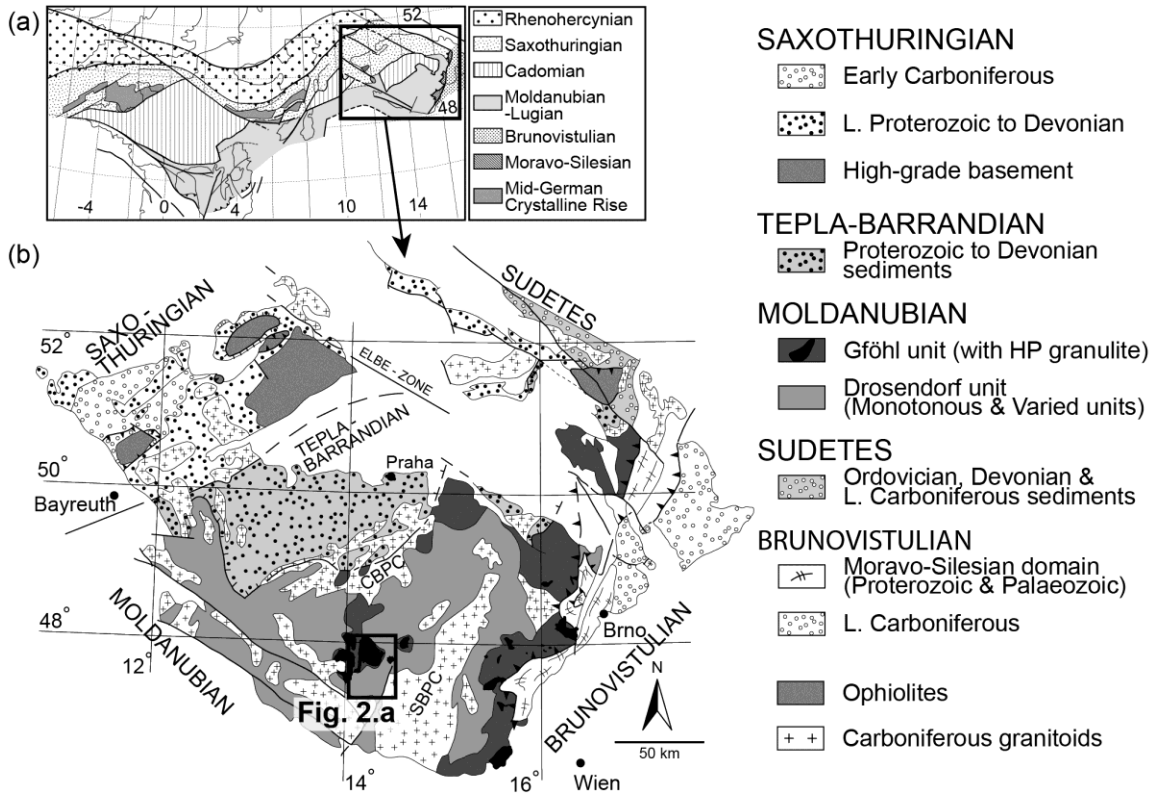

Fig. 1: Geology of the European Variscan Belt. (a) Simplified map of the main Variscan litho-tectonic domains (after Edel *et al.*, 2003). (b) Map of the Bohemian Massif (after Franke, 2000). Black rectangle shows the position of the study area (Fig. 2a). CBPC & SBPC = Central and South Bohemian plutonic complexes.

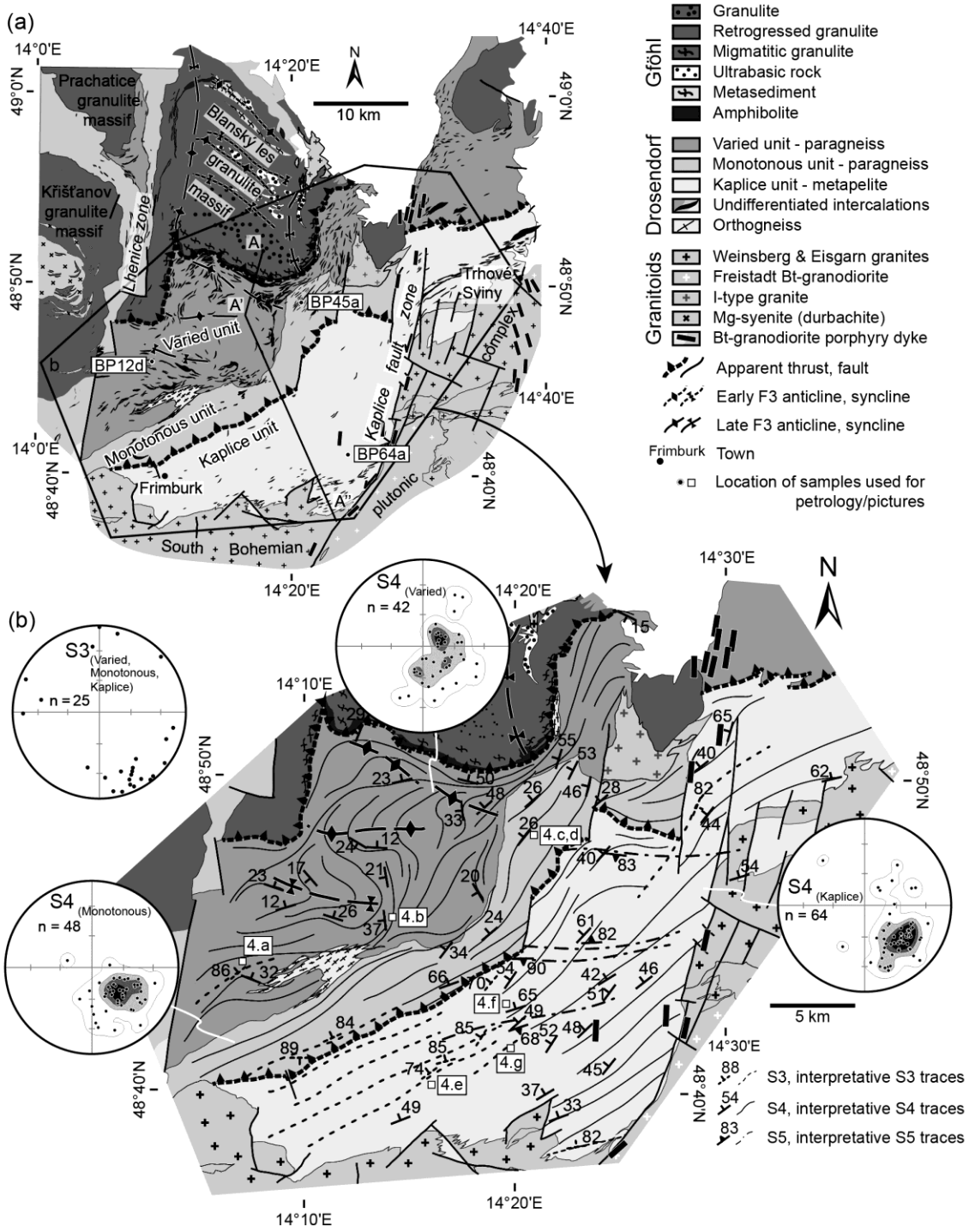

Fig. 2: Geology and structure of the study area. (a) Geological map. Lithologies are compiled from the Czech Geological Survey maps (scale 1:50 000). The location of samples used for petrology, and the position of the structural profile A−A'−A'' (Fig. 3) are indicated. (b) Structural map and stereonets for the S3 and S4 planar structures (equal-area, lower-hemisphere projection). The location of field photographs (Fig. 4) is indicated.

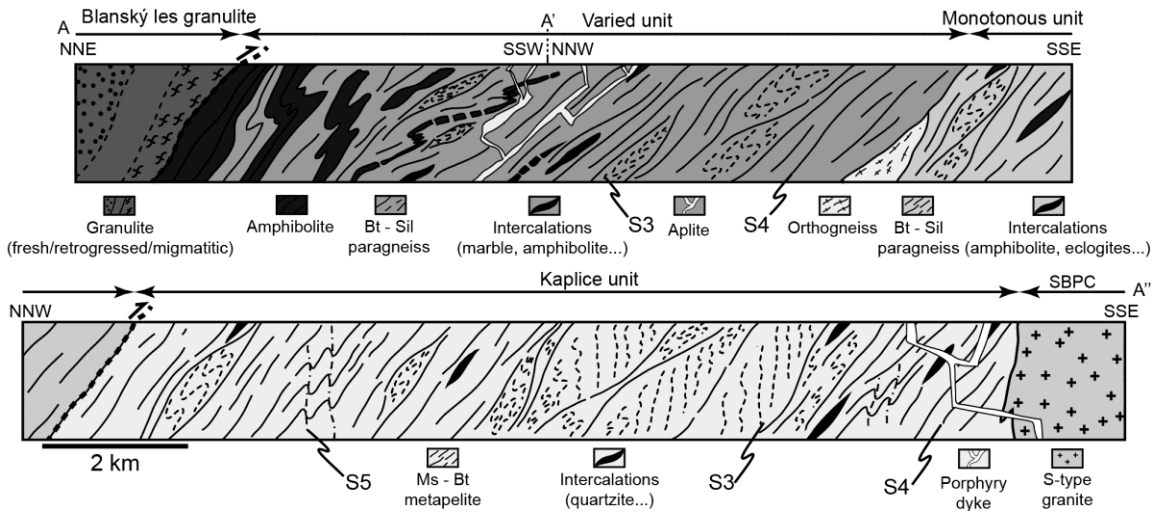

Fig. 3: Interpretative geological cross-section (location in Fig. 2a) showing the relationships between the subvertical fabric S3, the shallow-dipping fabric S4, and the late axial plane cleavage S5. Vertical axis not to scale. Western part of the cross-section modified after Franěk *et al.* (2006).

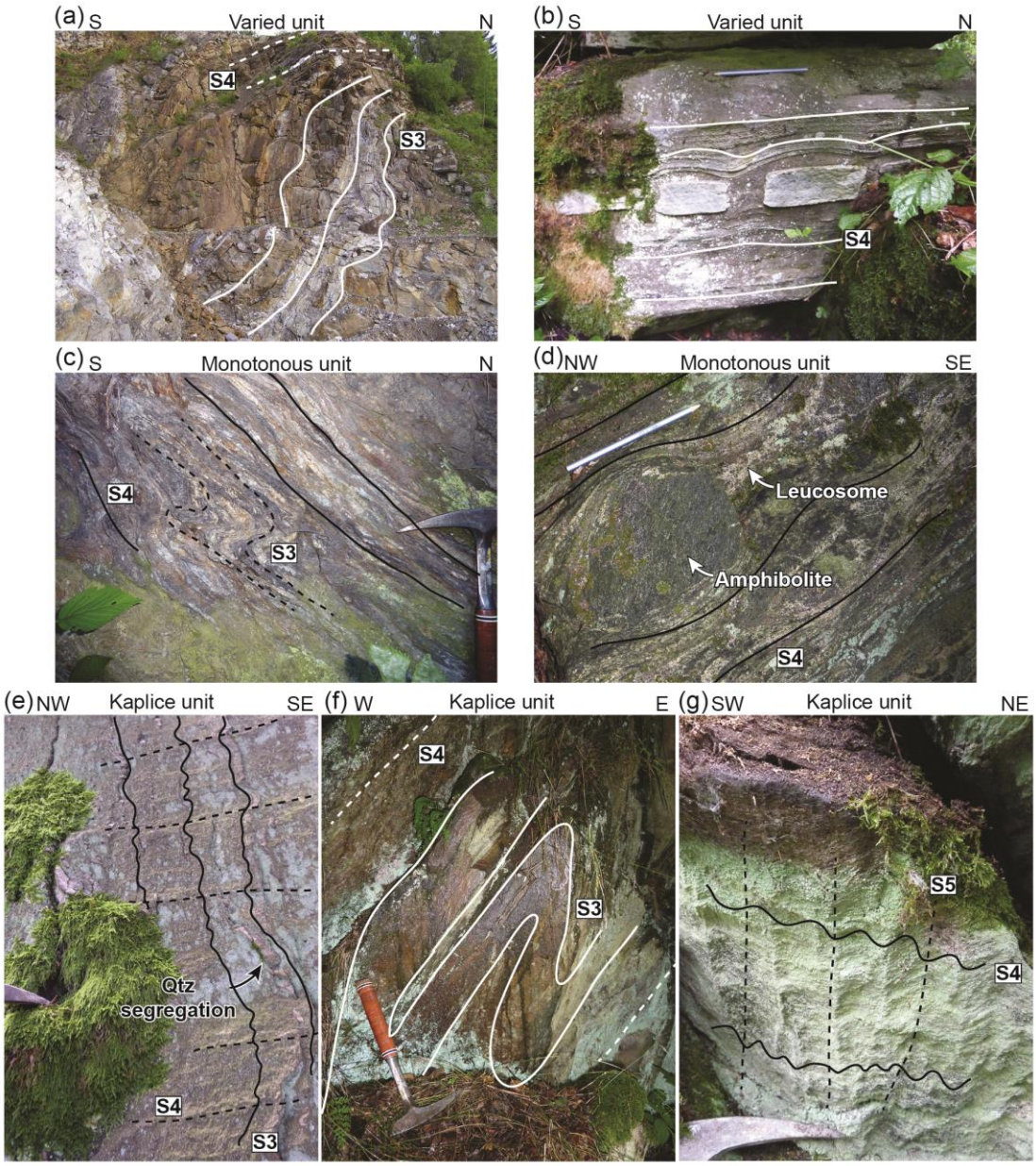

Fig. 4: Photographs of macroscopic structures. Varied unit: (a) paragneiss showing the S3 fabric weakly affected by F4 folds; (b) boudinage of a quartzite layer in marble due to D4 deformation. Monotonous unit: (c) paragneiss showing the transposition of the slightly migmatitic S3 fabric into the S4 fabric; (d) leucosome localized in the neck zone of a D4 amphibolite boudin in migmatitic paragneiss. Kaplice unit: (e) subvertical S3 foliation affected by F4 crenulation folds in micaschist; (f) relicts of the S3 foliation affected by isoclinal F4 folds in micaschist. (g) F5 crenulation folds and associated S5 cleavage in micaschist.

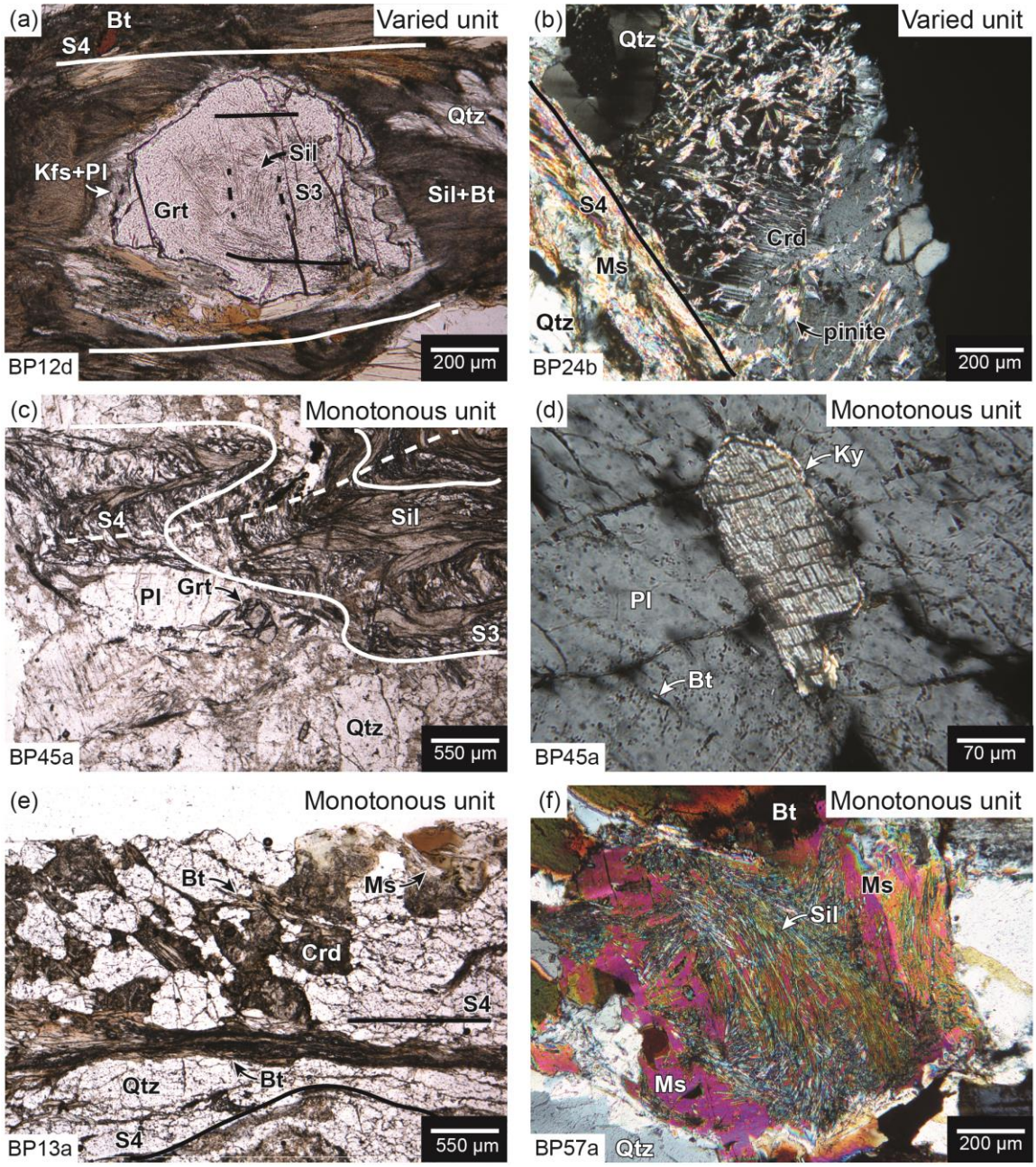

Fig. 5: Photomicrographs illustrating crystallization−deformation relationships in paragneiss from (a,b) the Varied unit and (c−f) the Monotonous unit. (a) Garnet with sillimanite inclusions oriented parallel to S3 in the core and parallel to S4 at the rim. The garnet is surrounded by a K-feldspar−plagioclase corona. (b) Pinitized cordierite porphyroblast with the characteristic "flame" twins. (c) S3 foliation marked by the alternation of quartz−plagioclase and sillimanite−biotite layers, and affected by F4 microfolds. (d) Close-up view of a kyanite inclusion in plagioclase from a garnet-bearing plagioclase−quartz layer (leucosome?). (e) Cordierite growing in sillimanite−biotite nests. (f) Sillimanite inclusions in a late muscovite porphyroblast.

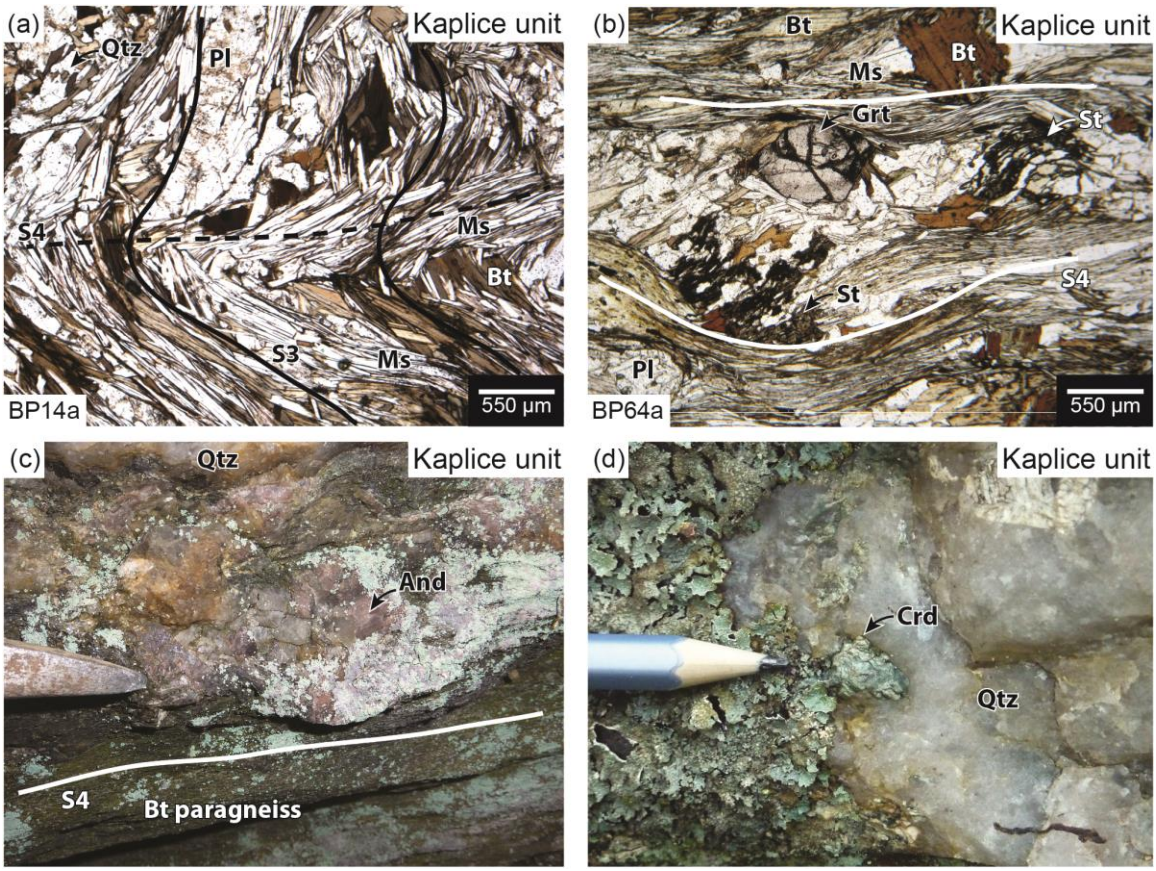

Fig. 6: Photomicrographs and field photographs showing the main metamorphic minerals in the Kaplice unit. (a) Typical aspect of the muscovite-bearing S3 foliation affected by F4 crenulation microfolds. (b) Garnet−staurolite−biotite−muscovite micaschist. Staurolite hosts quartz inclusion trails oblique to the surrounding S4 foliation. (c) Andalusite associated with a quartz segregation in micaschist. (d) Cordierite associated with a quartz segregation in micaschist.

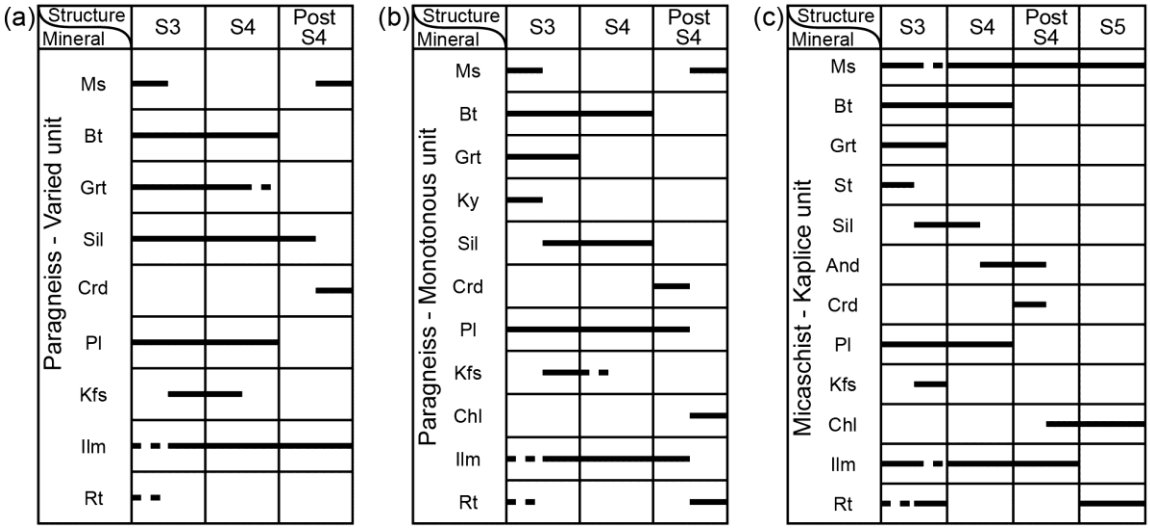

Fig. 7: Crystallization−deformation relationships. Quartz is always stable. See text for discussion.

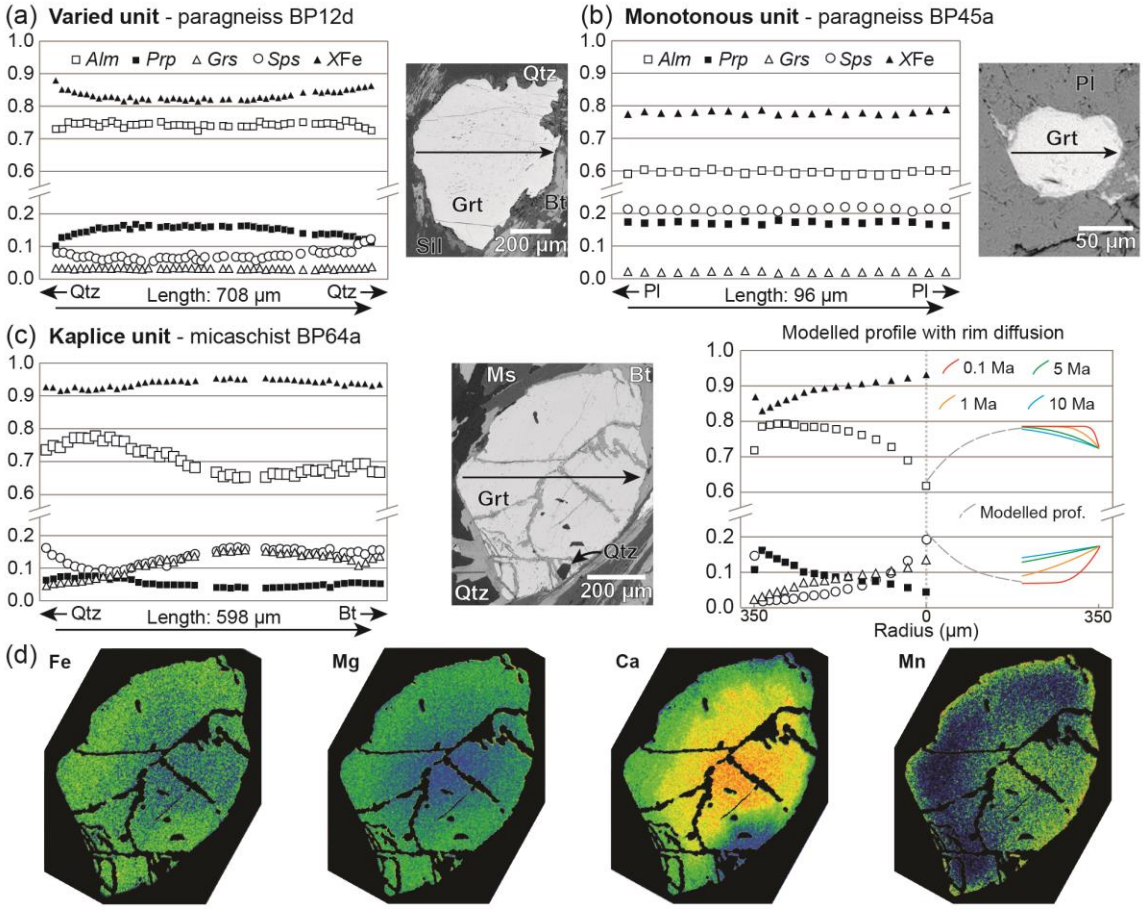

Fig. 8: Garnet composition in the different metasedimentary units. Measured garnet profiles for (a) the Varied unit and (b) the Monotonous unit. (c) Measured and modelled garnet profiles for the Kaplice unit. The modelled profile reflects a prograde path from 5.4 kbar/530°C to 7.1 kbar/660°C and rim re-equilibration at 4.9 kbar/647°C (path indicated in Fig. 11d). Diffusion of the *Alm* and *Sps* variables was allowed in the ~100µm-wide outermost part of the modelled profile for durations of 0.1, 1, 5 and 10 Ma. See text for further details. (d) Garnet compositional X-ray maps for the zoned garnet of the Kaplice unit shown in (c).

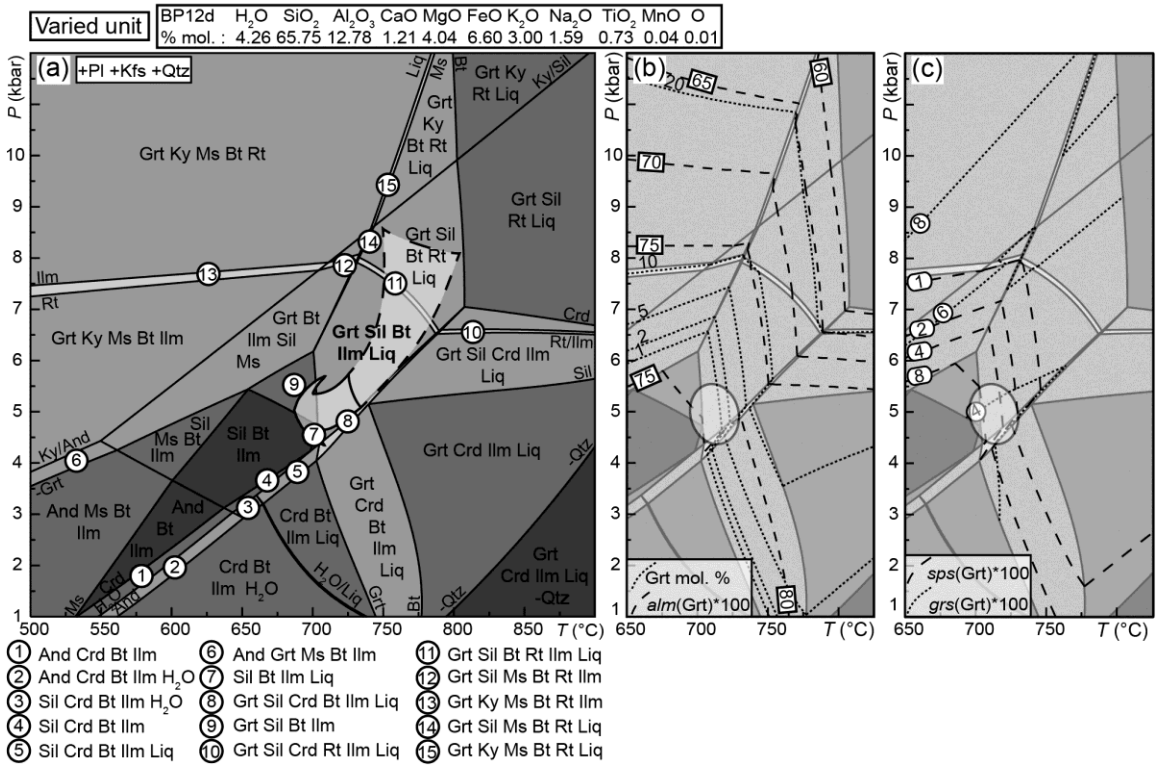

Fig. 9: (a) *P*−*T* pseudosection for Varied paragneiss sample BP12d (whole rock composition in molar percent adjusted to 100%). The arrow indicates the *P*−*T* evolution deduced from the observed matrix assemblage (in bold) and garnet composition. See text for further details. (b, c) Simplified part of the pseudosection contoured with garnet molar and compositional isopleths. Ellipses outline the probable equilibration area of garnet with the observed assemblage.

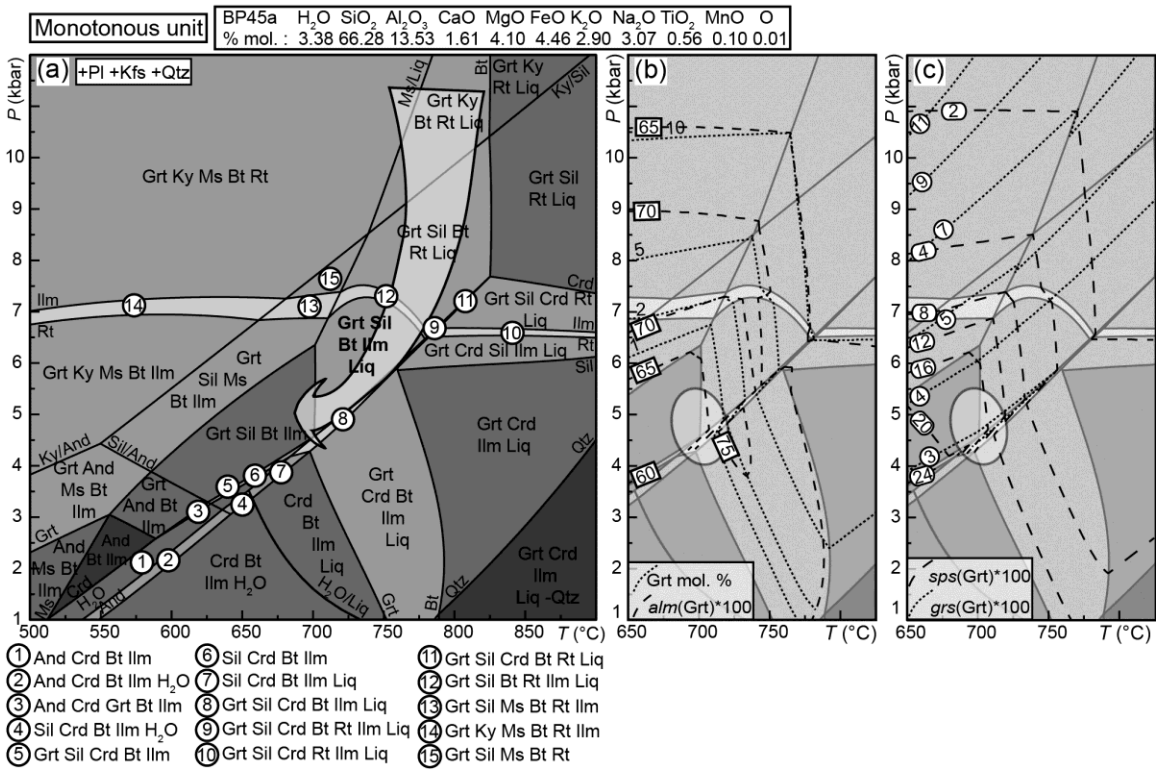

Fig. 10: (a) $P-T$ pseudosection for Monotonous paragneiss sample BP45a (whole rock composition in molar percent adjusted to 100%). The arrow indicates the $P-T$ evolution deduced from the succession of metamorphic minerals, the matrix assemblage (in bold) and garnet composition. See text for further details. (b, c) Simplified part of the pseudosection contoured with garnet molar and compositional isopleths. Ellipses outline the probable equilibration area of garnet with the observed assemblage.

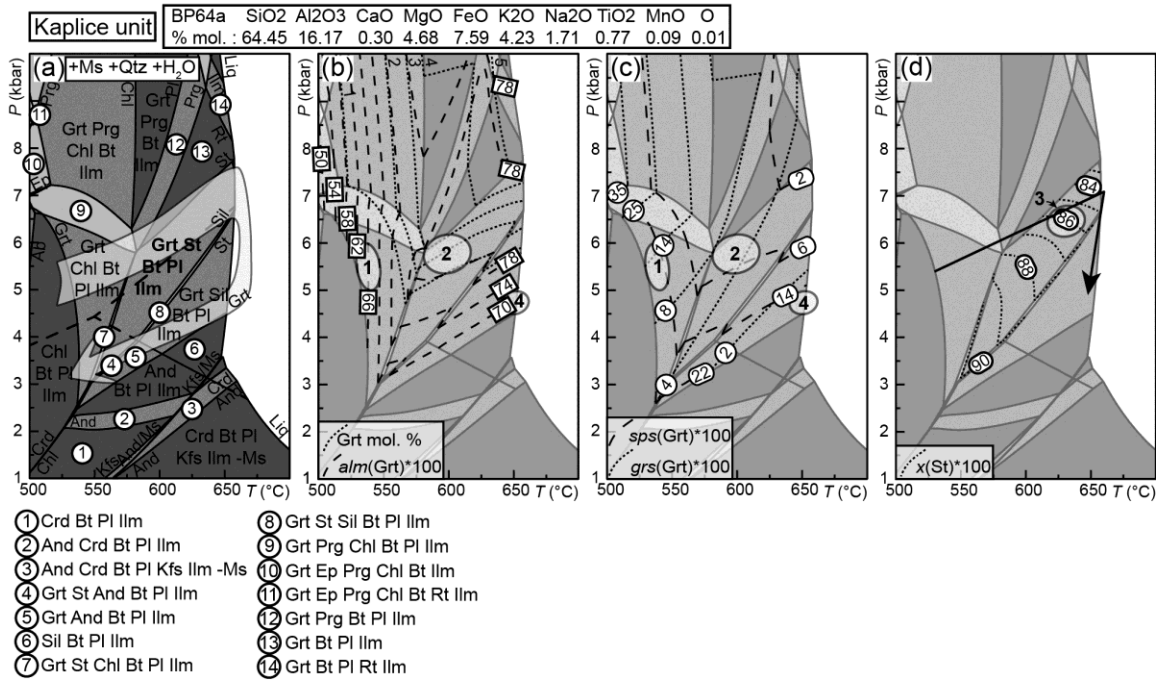

Fig. 11: (a) *P*−*T* pseudosection for Kaplice micaschist sample BP64a (whole rock composition in molar percent adjusted to 100%). The grey arrow indicates the *P*−*T* evolution deduced from the succession of metamorphic minerals, the matrix assemblage (in bold) and garnet and staurolite composition. See text for further details. (b−d) Simplified part of the pseudosection contoured with garnet molar isopleths and compositional isopleths for garnet and staurolite. Ellipses outline the probable equilibration area of garnet (from core to rim: circles 1, 2 and 4) and staurolite (circle 3). The black arrow indicates the *P*–*T* path used for the garnet modelling.

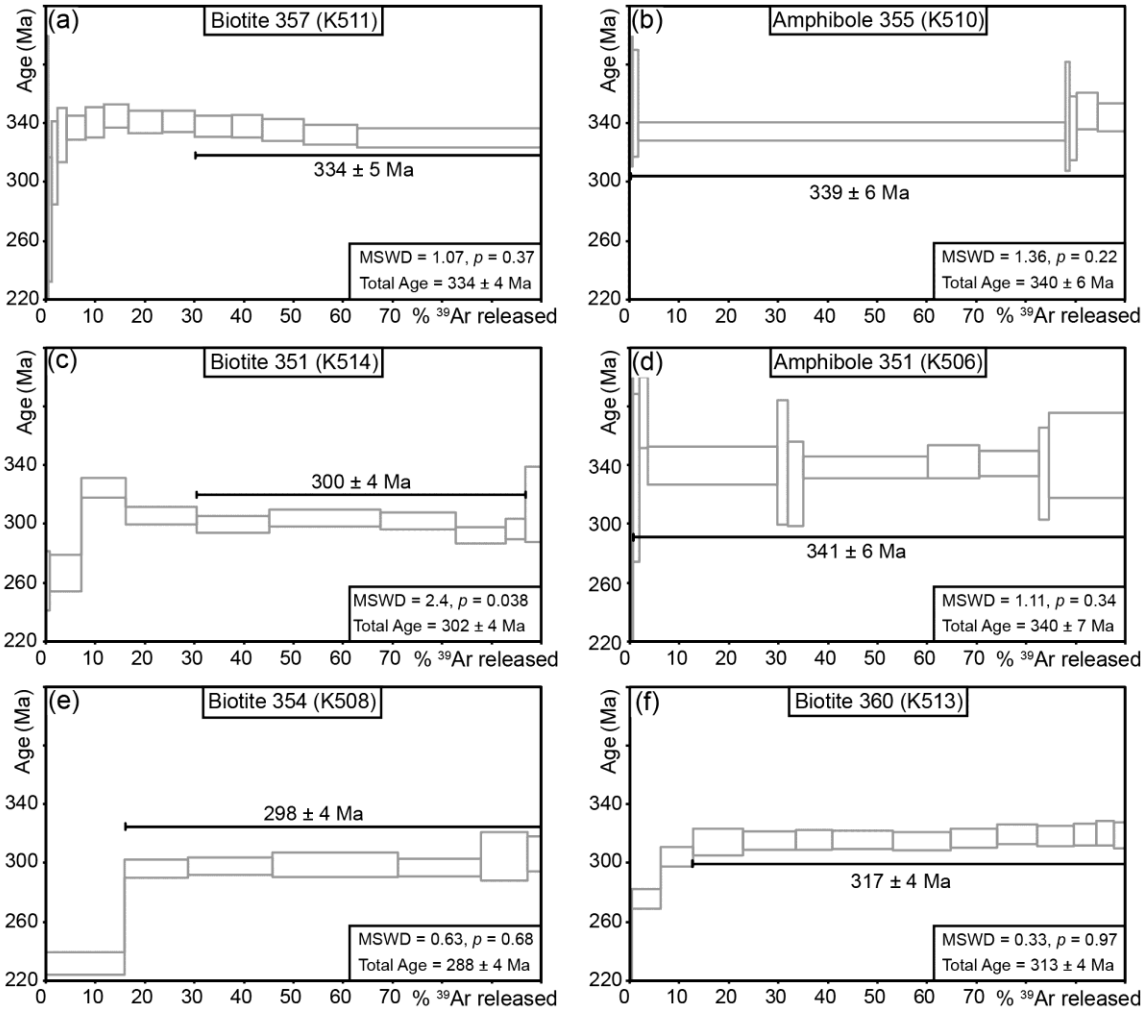

Fig. 12: ^{40}Ar–^{39}Ar step-release spectra for amphibole and biotite separated from (a) the Blanský les granulite, (b−d) the Varied unit and (g, f) the Kaplice unit. Steps used for the determination of plateau ages are indicated by the horizontal black lines. Sample locations are shown in Fig. 13 (labelled 10). Analysed mineral, sample name and analytical reference (in brackets) are given (top side) together with the mean square weighted deviation (MSWD) and probability of fit value (*p*-value) of the plateau age and the total isochron age (bottom right-hand side). Ages were regressed using the ArArCalc software (Koppers, 2002) and *p*-values using Isoplot v. 3.75 (Ludwig, 2012).

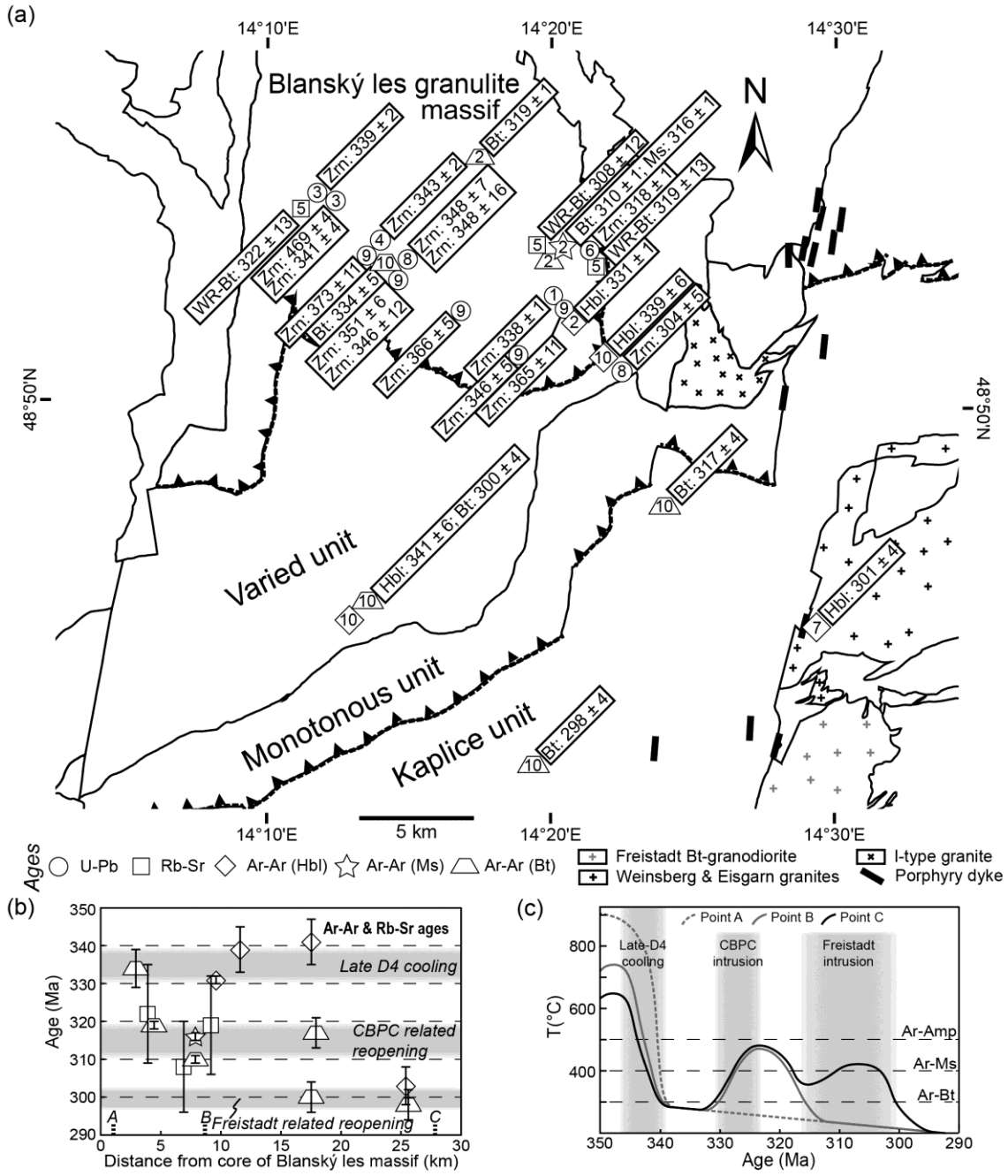

Fig. 13: Compilation of new and existing geochronological data for the study area. (a) Spatial distribution of metamorphic U−Pb zircon and ^{40}Ar–^{39}Ar ages. See Franěk *et al.* (2011a) for the complete U−Pb zircon age dataset. References: 1−Aftalion *et al.* (1989), 2− Košler *et al.* (1999), 3−Kröner *et al.* (2000), 4−Sláma *et al.* (2007), 5−Svojtka (2001), 6−Svojtka *et al.* (2002), 7−Vrána *et al.* (2005), 8−Wendt (1989), 9−Wendt *et al.* (1994), 10−this study. (b) Diagram illustrating the evolution of cooling ages with increasing distance from the granulite massif. (c) Schematic *T–t* curves for three points located: A–in the core of the granulite massif; B–at the granulite/Varied unit boundary; C–in the southeastern part of the study area.

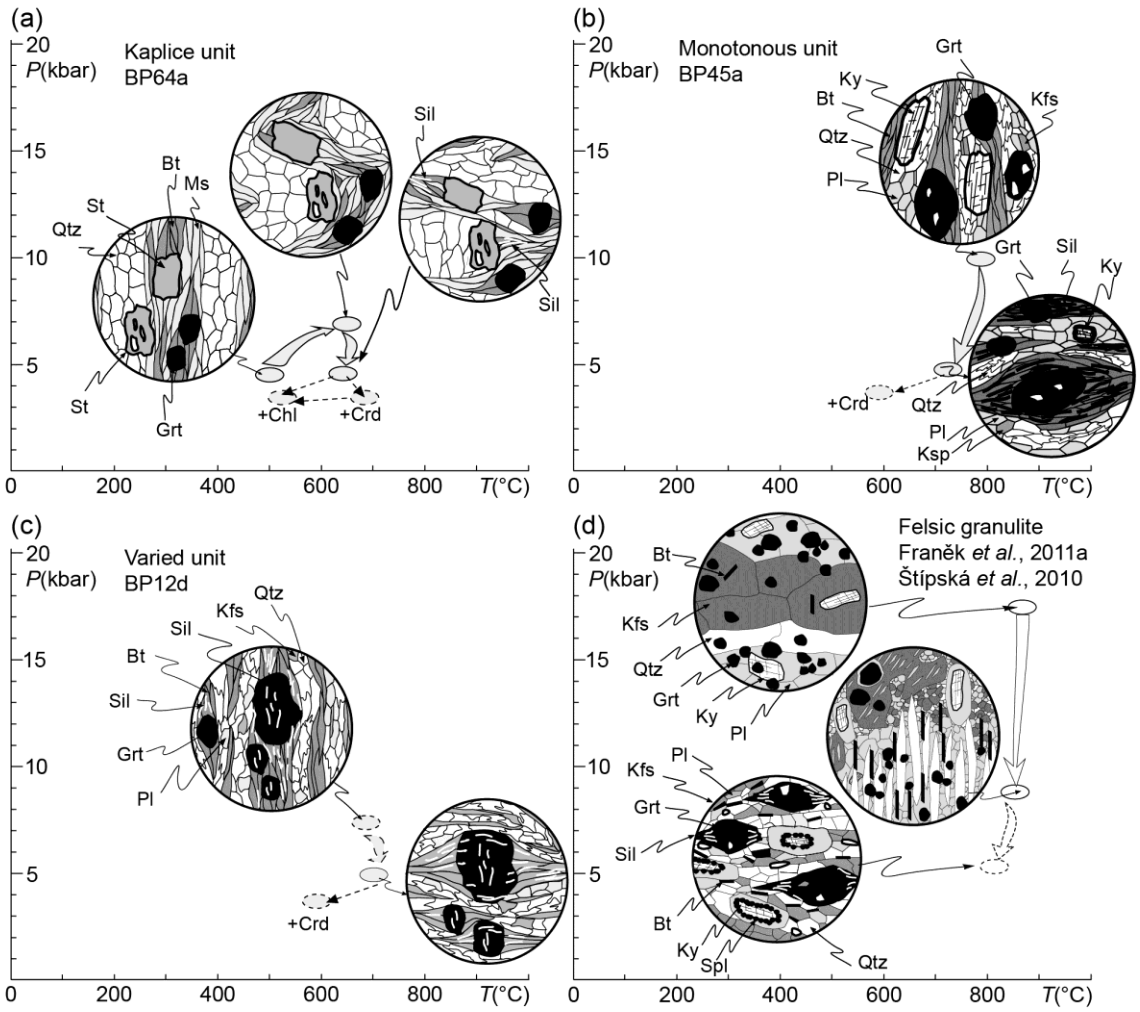

Fig. 14: Sketches summarizing the inferred *P*–*T* paths for (a) the Kaplice unit, (b) the Monotonous unit, (c) the Varied unit, and (d) the felsic granulite (after Franěk *et al.*, 2011a; Štípská *et al.*, 2010). See text for details.

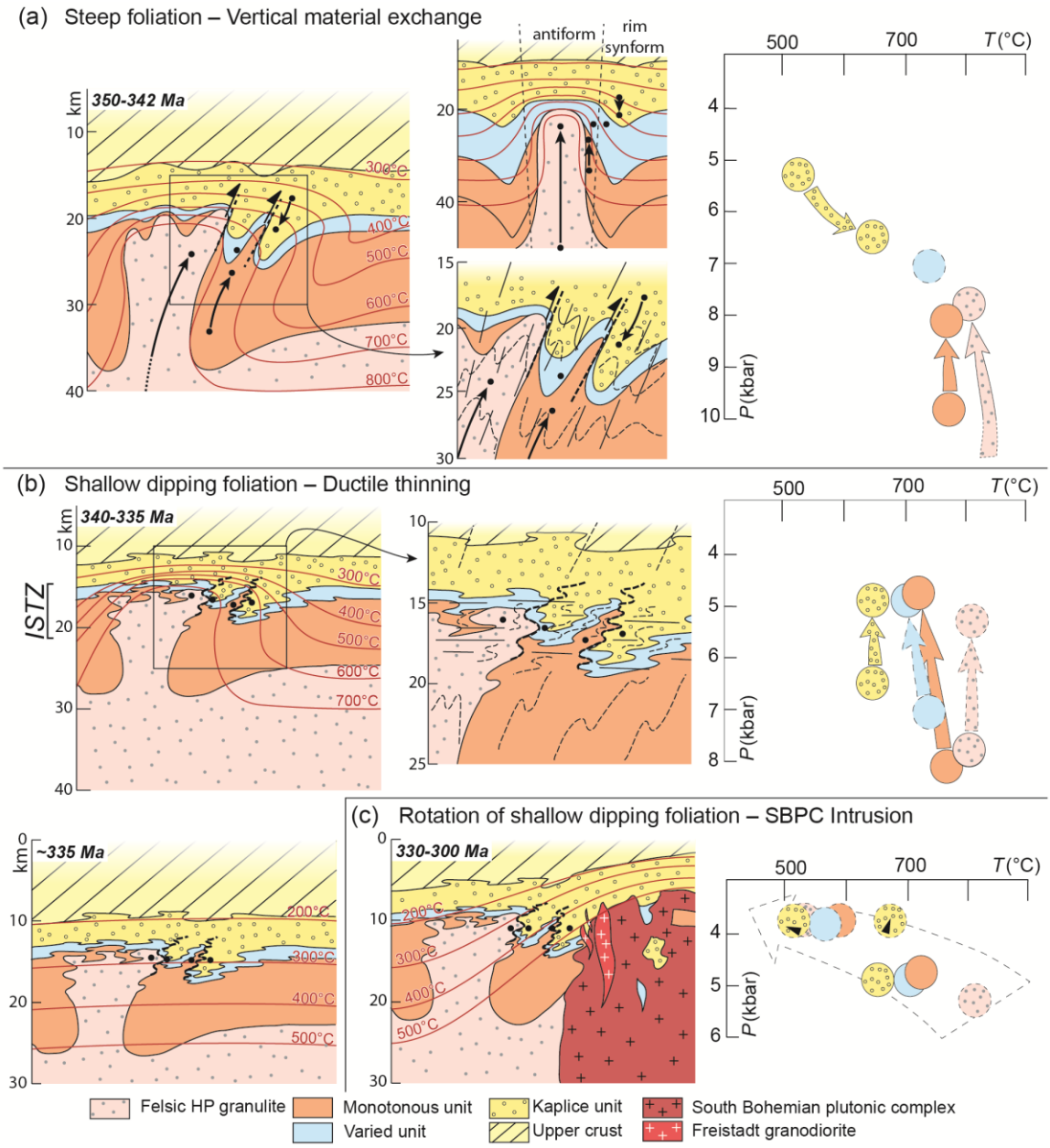

Fig. 15: Schematic view for the tectono-thermal evolution of the study area in a NW−SE ~50 km long section. *P–T* path of the granulite is after Franěk *et al.* (2011a). (a) Exhumation of the orogenic lower and middle crust and synchronous burial of the orogenic upper crust between 350 and 342 Ma. (b) Ductile thinning and associated exhumation of the lower, middle and upper crustal rocks followed by a fast cooling. (c) Re-heating by the late intrusions of the South Bohemian plutonic complex.

Lithology	Varied paragneiss (BP12d)					Monotonous paragneiss (BP45a)					Kaplice micaschist (BP64a)							
Mineral	Grt		Pl	Kfs	Bt	Grt	Pl	Kfs	Bt	Ms	Grt			Pl	Kfs	Bt	Ms	St
Position	core	rim	mat.	mat.	mat.	mat.	rim	incl. Pl	mat.	mat.	core	int. rim	ext. rim	mat.	mat.	mat.	mat.	mat.
An. Name	s33	s47	s01	s11	p16	s34	p16	s15	s22	s21	s33	s10	s02	p37	s14	p32	s04	s101
Wt%																		
SiO_2	37.66	37.00	60.46	64.81	35.21	36.56	63.09	64.29	36.45	46.10	36.47	36.40	36.01	66.18	63.33	34.08	47.46	26.83
TiO_2	0.00	0.07	0.00	0.00	3.32	0.30	0.00	0.05	2.59	2.72	0.06	0.11	0.06	0.00	0.00	1.61	0.35	0.69
Al_2O_3	21.25	20.80	24.92	18.80	19.52	21.07	23.67	18.93	21.11	34.69	20.31	20.36	20.21	21.80	18.23	19.43	37.20	55.06
FeO	35.19	34.51	0.40	0.24	19.55	26.51	0.00	0.25	17.01	1.33	31.47	36.41	34.74	0.00	1.51	22.17	1.19	12.01
MnO	2.43	3.66	0.08	0.00	0.15	10.00	0.00	0.00	0.54	0.08	6.42	3.69	5.78	0.00	0.00	0.23	0.07	0.56
MgO	3.97	2.85	0.07	0.07	8.74	3.47	0.00	0.13	9.56	0.97	0.89	1.56	1.50	0.00	0.38	7.77	0.44	1.12
CaO	1.19	1.11	6.86	0.23	0.00	0.74	4.48	0.06	0.06	0.00	5.01	2.55	1.81	1.95	0.25	0.00	0.17	0.04
Na_2O	0.09	0.11	7.04	1.38	0.11	0.00	9.22	0.53	0.16	0.50	0.10	0.00	0.00	10.83	0.08	0.11	1.47	0.00
K_2O	0.03	0.03	0.13	15.27	9.81	0.03	0.11	15.96	10.03	10.70	0.00	0.04	0.00	0.06	16.25	9.14	9.73	0.06
ZnO	n.a.	n.a.	n.a.	n.a.	n.a.	n.a.	n.a.	n.a.	n.a.	n.a.	n.a.	n.a.	n.a.	n.a.	n.a.	n.a.	n.a.	1.39
Total	101.81	100.14	99.96	100.80	96.41	98.68	100.57	100.20	97.51	97.09	100.73	101.12	100.11	100.82	100.03	94.54	98.08	97.76
Cations/Charge	8/24	8/24	5/16	5/16	8/24	8/24	5/16	5/16	8/24	7/24	8/24	8/24	8/24	5/16	5/16	8/24	7/24	30/48
Si	2.97	2.98	2.71	2.95	2.74	2.98	2.77	2.96	2.77	3.04	2.94	2.94	2.94	2.88	2.94	2.72	3.06	7.62
Ti	0.00	0.00	0.00	0.00	0.19	0.02	0.00	0.00	0.15	0.13	0.00	0.01	0.00	0.00	0.00	0.10	0.02	0.15
Al	1.97	1.98	1.32	1.01	1.79	2.02	1.23	1.03	1.89	2.69	1.93	1.94	1.94	1.12	1.00	1.82	2.82	18.44
Fe^{3+}	0.11	0.07	0.00	0.01	0.00	0.00	0.00	0.01	0.00	0.00	0.19	0.18	0.17	0.00	0.06	0.00	0.01	0.00
Fe^{2+}	2.20	2.26	0.01	0.00	1.27	1.80	0.00	0.00	1.08	0.07	1.94	2.27	2.20	0.00	0.00	1.48	0.05	2.85
Mn	0.16	0.25	0.00	0.00	0.01	0.69	0.00	0.00	0.03	0.00	0.44	0.25	0.40	0.00	0.00	0.02	0.00	0.13
Mg	0.47	0.34	0.00	0.00	1.01	0.42	0.00	0.01	1.08	0.10	0.11	0.19	0.18	0.00	0.03	0.92	0.04	0.47
Ca	0.10	0.10	0.33	0.01	0.00	0.07	0.21	0.00	0.00	0.00	0.43	0.22	0.16	0.09	0.01	0.00	0.01	0.01
Na	0.01	0.02	0.61	0.12	0.02	0.00	0.78	0.05	0.02	0.06	0.02	0.00	0.00	0.91	0.01	0.02	0.18	0.00
K	0.00	0.00	0.01	0.89	0.97	0.00	0.01	0.94	0.97	0.90	0.00	0.00	0.00	0.00	0.96	0.93	0.80	0.02
Zn	n.a.	n.a.	n.a.	n.a.	n.a.	n.a.	n.a.	n.a.	n.a.	n.a.	n.a.	n.a.	n.a.	n.a.	n.a.	n.a.	n.a.	0.29
H	0	0	0	0	2	0	0	0	2	2	0	0	0	0	0	2	2	2
Total	8.00	8.00	5.00	5.00	8.00	8.00	5.00	5.00	8.00	7.00	8.00	8.00	8.00	5.00	5.00	8.01	7.00	30.00
X Fe/*Ab*	0.83	0.87	0.64	0.12	0.56	0.81	0.78	0.05	0.50		0.95	0.93	0.93	0.91	0.01	0.62		0.86
Alm/An	0.75	0.77	0.35	0.01		0.61	0.21	0.00			0.66	0.78	0.75	0.09	0.01			
Prp/Or	0.16	0.12	0.01	0.87		0.14	0.01	0.95			0.04	0.06	0.06	0.00	0.98			
Grs	0.03	0.03				0.02					0.15	0.08	0.05					
Sps	0.06	0.08				0.23					0.15	0.09	0.14					

Table 1: Representative mineral analyses for samples BP12d (Varied unit), BP45a (Monotonous unit) and BP64a (Kaplice unit). Analysis names starting with “s” were performed in Strasbourg, starting with “p” were performed in Prague.

	wt%	SiO_2	Al_2O_3	Fe_2O_3	MgO	CaO	Na_2O	K_2O	TiO_2	MnO
Varied unit	BP12d	59.94	19.76	8.00	2.47	1.30	1.49	4.28	0.88	0.04
Monotonous unit	BP45a	59.26	20.52	5.30	2.46	1.35	2.83	4.06	0.67	0.10
Kaplice unit	BP64a	53.79	22.89	8.42	2.62	0.23	1.47	5.53	0.85	0.09

Table 2: Major element concentrations (in weight percent) in samples used for mineral equilibria modelling (from whole rock analyses by ICP-AES).